

**SAGE III Algorithm Theoretical Basis Document (ATBD)
Transmission Level 1B Products**



Compiled by the SAGE III ATBD Team

**LaRC 475-00-108
Version 2.1
26 March 2002**

TABLE OF Contents

1.0	INTRODUCTION	1
1.1	PURPOSE	1
1.2	APPLICABLE DOCUMENTS.....	1
1.2.1	<i>Controlling Documents</i>	1
1.2.2	<i>SAGE III ATDB Reference Documents</i>	2
1.3	REVISION HISTORY	2
1.4	CONTRIBUTING AUTHORS	3
1.5	SAGE III STANDARD DATA PRODUCTS	5
2.0	BACKGROUND	6
2.1	EXPERIMENTAL OBJECTIVES	6
2.2	NEED FOR THE SAGE III MEASUREMENTS	7
2.3	HERITAGE	7
3.0	ALGORITHM DESCRIPTION	8
3.1	INTRODUCTION	8
3.1.1	<i>Physical Description</i>	8
3.1.2	<i>The Forward Problem</i>	11
3.2	RETRIEVAL ALGORITHM DESCRIPTION	12
3.2.1	<i>Overview and Assumptions</i>	12
3.2.2	<i>Algorithm Mathematical Description</i>	16
3.2.3	<i>Algorithm Description</i>	18
3.3	ALGORITHM TESTING REQUIREMENTS.....	26
3.4	VALIDATION PLAN.....	26
3.5	QUALITY CONTROL AND DIAGNOSTICS	26
3.6	EXCEPTION HANDLING	26
4.0	REFERENCES	28
APPENDIX A. SAGE III INSTRUMENT DESCRIPTION		30
APPENDIX B. ATMOSPHERIC INHOMOGENEITY		36
APPENDIX C. MOLECULAR ABSORPTION CROSS-SECTIONS: SPECTROSCOPIC CONSIDERATIONS FOR SAGE III		39
C.1	INTRODUCTION	39
C.2	SPECIES SPECIFIC INFORMATION	39
C.2.1	<i>Ozone</i>	39
C.2.2	<i>Nitrogen Dioxide</i>	44
C.2.3	<i>Oxygen</i>	46
C.2.4	<i>Water Vapor</i>	48
C.2.5	<i>The Nitrate Free Radical NO₃</i>	50
C.2.6	<i>Symmetric Chlorine Dioxide OClO</i>	52

CHANGE RECORD PAGE

ISSUE	DATE	PAGES AFFECTED	DESCRIPTION
Baseline	November 10, 2000	All	
Version 2.1	March 26, 2002	Section 1.5; p. 3 Table 1.6.1; p.5	Added contributing authors Removed references to mixing ratio profiles

1.0 Introduction

The Stratospheric Aerosol and Gas Experiment III (SAGE III) is a critical part of the Earth Observing System (EOS). The EOS mission is to develop an understanding of the total Earth system and the effects of natural and human-induced changes on the global environment. SAGE III provides limb occultation measurements with a flexible instrument design that permits on orbit reprogramming and channel selection with up to 809 channels spanning the ultraviolet, visible, and near infrared (280-1040 nm). Solar observations will provide high resolution vertical profiles of multi-wavelength aerosol extinction, the molecular density of ozone, nitrogen dioxide, and water vapor, as well as profiles of temperature, pressure, and cloud presence. In addition, the inclusion of a repositionable solar attenuator will allow lunar occultation observations that will improve the geographic coverage and permit measurements of nitrogen trioxide and chlorine dioxide in addition to ozone, nitrogen dioxide, water vapor, and pressure.

1.1 Purpose

This Algorithm Theoretical Basis Document (ATBD) describes the algorithm used to produce the Stratospheric Aerosol and Gas Experiment III (SAGE III) level 1B1 atmospheric slant path transmission products. The main function of this SAGE III level 1B1 processing algorithm is to convert the radiometric measurements from the SAGE III instrument in the form of binary counts from the different channels into atmospheric slant path transmittance at the specific location in the atmosphere for the different spectral wavelengths. The SAGE III level 1B1 transmission data products will be the input data for the processing to produce the SAGE III solar occultation level 2 data products.

1.2 Applicable Documents

1.2.1 Controlling Documents

EOS Science Plan, NASA HQ EOS, January 1999.

Mission to Planet Earth Strategic Enterprise Plan 1996-2002, NASA HQ EOS, May 1996.

Execution Phase Project Plan for Earth Observing System (EOS), GSFC 170-01-01, Rev. A., May 1995.

1.2.2 SAGE III ATDB Reference Documents

SAGE III Algorithm Theoretical Basis Document: Transmission Data Products, LaRC 475-00-108, February 2000.

SAGE III Algorithm Theoretical Basis Document: Cloud Presence Data Products, LaRC 475-00-106, February 2000.

SAGE III Algorithm Theoretical Basis Document: Solar and Lunar Algorithm, LaRC 475-00-109, November 2000.

1.3 Revision History

The original version of this document was dated November 15, 1996. Version 1.1 was released on 15 April 1997. Version 1.2, was released on 18 February 2000. Version 2.0 was released on 10 November 2000. This release, version 2.1, is dated March 2002.

1.4 Contributing Authors

The SAGE III ATBDs were drafted by a team of SAGE III science team members and SAGE III science cadre, led by one of the science team members. The entire team participated in oral and written revisions of the methodology and documentation as part of the SAGE III science team meetings and research activities.

Contributing Authors	Affiliation
Colette Brogniez	University de Lille, France
Er-Woon Chiou	SAIC
William P. Chu	NASA Langley Research Center
Albert A. Chernikov	Central Aerological Observatory
Derek M. Cunnold	Georgia Tech
John DeLuisi	NOAA
Philip A. Durkee	Naval Postgraduate School
Nikolai F. Elansky	Russian Academy of Science
Benjamin M. Herman	University of Arizona
Peter V. Hobbs	University of Washington
Geoff S. Kent	Science and Technology Corporation
Jacqueline Lenoble	University de Lille, France
M. P. McCormick, Principal Investigator	Hampton University
Hope A. Michelsen	AER
Alvin J. Miller	NOAA/NCEPS
Volker Mohnen	State University of New York at Albany
Randy Moore	SAIC
Michael C. Pitts	NASA Langley Research Center
Lamont R. Poole	NASA Langley Research Center
Venkatachalam Ramaswamy	Princeton University
David Rind	Goddard Institute for Space Studies
David Risley	SAIC
Michael W. Rowland	SAIC
Philip B. Russell	NASA Ames Research Center
Vinod K. Saxena	North Carolina State University
Eric P. Shettle	Naval Research Laboratory
Victor E. Sothcott	SAIC
Ghassan Taha	University of Arizona
Larry W. Thomason	NASA Langley Research Center
Charles R. Trepte	NASA Langley Research Center
Gabor Vali	University of Wyoming
Lelia B. Vann	NASA Langley Research Center
Robert E. Veiga	SAIC
Pi-Huan Wang	Science and Technology Corporation
Steven C. Wofsy	Harvard University
David C. Woods	NASA Langley Research Center

Joseph M. Zawodny	NASA Langley Research Center
-------------------	------------------------------

Technical assistance was provided by Jackie Bumgardner, Kathy Drummond and Susan Walters.

1.5 SAGE III Standard Data Products

Table 1.5.1 SAGE III standard data products

PRODUCT NAME	UNCERTAINTY Systematic :: Precision	TEMPORAL RESOLUTION	HORIZONTAL Resolution :: Coverage	VERTICAL Resolution :: Coverage
Level 1B Transmission (≤ 80 wavelengths) Solar Events	0.05% :: 0.05%	1/(2 minutes), 30/day	<2 x <1 deg :: Global	0.5 km :: 0-100 km
Aerosol Extinction Stratospheric Optical Depth (at 9 wavelength bands), Aerosol to molecular/extinction ratio at 1020 nm (solar only)	5% :: 5%	1/(2 minutes), 30/day	<2 x <1 deg :: Global	0.5 km :: 0-40 km
O ₃ Concentration Slant Path Col. Density	6% :: 5%	1/(2 minutes), 30/day	<2 x <1 deg :: Global	0.5 km :: 6-85 km 0.5 km :: 50-85 km
NO ₂ Concentration Slant Path Col. Density	10% :: 15%	1/(2 minutes), 30/day	<2 x <1 deg :: Global	0.5 km :: 10-50 km 0.5 km :: 10-50 km
H ₂ O Concentration	10% :: 15%	1/(2 minutes), 30/day	<2 x <1 deg :: Global	0.5 km :: 0-50 km
NO ₃ (Lunar Only) Concentration	10% :: 10%	1/(2 minutes), ≤ 30 /day	<2 x <1 deg :: Global	0.5 km :: 20-55 km
OCIO (Lunar Only) Concentration	25% :: 20%	1/(2 minutes), ≤ 30 /day	<2 x <1 deg :: Global	0.5 km :: 15-25 km
Pressure	2% :: 2%	1/(2 minutes), 30/day	<2 x <1 deg :: Global	0.5 km :: 0-85 km 1000-0.004 hPa
Temperature Profile	2K :: 2K	1/(2 minutes), 30/day	<2 x <1 deg :: Global	0.5 km :: 0-85 km
Cloud Presence	N/A	1/(2 minutes), 30/day	<2 x <1 deg :: Global	0.5 km :: 6-30 km

2.0 Background

SAGE III is the fifth generation of solar occultation instruments designed to measure atmospheric aerosols and gaseous species in the atmosphere. The solar occultation method employs the attenuation of the Sun's rays as observed through the limb of the Earth's atmosphere to determine the vertical distribution of important atmospheric constituents. Measurements are made during each sunrise and sunset (an "event") encountered by the spacecraft (~30/day). This method is well-suited for long-term monitoring of trends and variability in key species such as ozone since the instrument is recalibrated during each event. The instrument concept originated as a hand-held, single wavelength sunphotometer (Stratospheric Aerosol Measurement or SAM) which was flown onboard an Apollo mission in 1975 [Pepin *et al.*, 1977]. SAM II was a one wavelength (1000 nm) instrument which operated on Nimbus-7 between 1978 and 1994 [McCormick *et al.*, 1979, 1981]. The Stratospheric Aerosol and Gas Experiment (SAGE) operated on the Application Explorer Mission 2 (AEM-2) spacecraft between 1979 and 1981. This instrument made measurements at 4 wavelengths and measured molecular density profiles of O₃ and NO₂ in addition to aerosol extinction at 2 wavelengths (450 and 1000 nm) [McCormick *et al.*, 1979]. SAGE II has operated on the Earth Radiation Budget Satellite (ERBS) since 1984 and makes measurements at 7 wavelengths. In addition to the species measured by SAGE, SAGE II measures the molecular density profile of H₂O and aerosol extinction at 4 wavelengths (385, 453, 525 and 1020 nm) (Mauldin, 1985 McCormick, 1987). In SAGE III, a charged coupled device (CCD) linear array provides spectral coverage from 280 to 1040 nm. In addition, a single photodiode adds aerosol extinction measurements at 1550 nm. [McCormick *et al.*, 1991; Mauldin *et al.*, 1989; McCormick *et al.*, 1993]. A repositionable solar attenuator will permit both solar and lunar occultation measurements, increasing the geographical coverage and allowing for the detection of nitrogen trioxide and chlorine dioxide. The incorporation of the CCD array will permit the measurement of gaseous species from multichannel absorption signatures simplifying the retrieval process, and 16-bit digitization will improve the precision and altitude range of the measurements.

2.1 Experimental Objectives

The science objectives to be accomplished by SAGE III are:

- Retrieve global profiles of atmospheric aerosol extinction, temperature, and pressure and molecular density profiles of ozone, water vapor, nitrogen dioxide, nitrogen trioxide, and chlorine dioxide with 0.5 km vertical resolution.
- Characterize tropospheric as well as stratospheric clouds and investigate their effects on the Earth's environment, including radiative, microphysical, and chemical interactions.
- Determine long-term trends in gaseous species and temperature.

- Provide atmospheric data essential for the interpretation and calibration of other satellite sensors, including EOS instruments.
- Investigate the spatial and temporal variability of these species in order to determine their role in climate processes, biogeochemical cycles, and the hydrological cycle.

2.2 Need For the SAGE III Measurements

The SAGE III experiment will provide output data products consisting of global vertical distributions of aerosol extinction at seven wavelengths, O₃, H₂O, NO₂, NO₃, OCIO, clouds, and temperature and pressure. Aerosols, O₃, clouds, and H₂O all play an important role in the radiative balance of the Earth-atmospheric system, while O₃, NO₂, NO₃, and OCIO are key molecules involved with the ozone chemistry in the stratosphere. SAGE III measurements are important components of the Earth Observation System (EOS) in monitoring elements of global change. The scientific importance of the atmospheric constituents and parameters, such as temperature, measured by SAGE III are discussed in the respective Algorithm Theoretical Basic Documents (See Section 1.3) and will not be discussed here.

This document presents the algorithm used to produce the intermediate product from the SAGE III measurements: the atmospheric slant path transmission profiles. These data products are used by the SAGE III inversion algorithm to generate the different species vertical profiles.

2.3 Heritage

SAGE III is the fifth generation of the solar occultation instrument that was designed to measure atmospheric aerosols and gaseous species in the atmosphere. It has evolved from a simple hand-held, one channel, manually operated sunphotometer SAM which was flown onboard the Apollo capsule in 1975 [Pepin *et al.*, 1977]; to an autonomous operated one channel instrument SAM II that flew on NIMBUS-7 from 1978 to 1994; then, to a four channel instrument SAGE I onboard the AEM-2 spacecraft which operated from 1979 to 1981 [McCormick *et al.*, 1979]; and then to a seven channel SAGE II instrument on the ERBS spacecraft that has operated from 1984 to the present [Mauldin *et al.*, 1985]. Each new generation instrument, in addition to being more complex in instrument design, has also added gaseous measurements of O₃, NO₂, H₂O, and improved aerosol information by the measurement of aerosol extinction properties at more wavelengths. The current SAGE III design utilizes an 809 element CCD linear array detector to provide spectral coverage from 280 nm to 1040 nm, together with a single photodiode detector at 1550 nm to expand the aerosol measurement in order to improved sensitivity to large aerosol particles [McCormick *et al.*, 1993]. A detailed description of the SAGE III instrument can be found in Appendix A.

3.0 Algorithm Description

3.1 Introduction

3.1.1 Physical Description

SAGE III is designed to measure the attenuation of solar radiation by the Earth's atmosphere due to scattering and absorption by atmospheric constituents during each sunrise and sunset encountered by its spaceborne platform. In addition, SAGE III will make measurements during moonrise and moonset when the atmosphere is not directly illuminated by the Sun. SAGE III consists of three subsystems: the pointing, the imaging, and the spectrometer subsystems. The pointing subsystem consists of a scan mirror which acquires the radiant target (either the Sun or the Moon), and performs vertical scanning (with respect to the Earth's horizon) across the target. A measurement is considered to occur at the point along the line of sight (LOS) from the instrument to the target at which it comes closest to the Earth's surface (i.e., the sub-tangent point). The altitude of that point above the Earth's surface is commonly referred to as the tangent altitude. The imaging subsystem produces a focused image of the target at a focal plane where the "science" aperture, that defines the instrument's instantaneous field of view (IFOV), is situated. The SAGE III IFOV is 30 arcseconds in the vertical direction which translates to approximately 0.5 km at the tangent altitude. The spectrometer subsystem is situated behind the science aperture and consists of an 809-element CCD to measure solar radiation from 280 to 1040 nm with 1 to 2 nm spectral resolution. An additional photodetector is used to measure radiation at 1550 nm.

The viewing geometry of a solar occultation event is illustrated in Figure 3.1.1. During an event, the spacecraft motion relative to the Sun's (or Moon's) location permit the measurement of atmospheric transmission at tangent altitudes from the Earth's surface to well above the atmosphere. Since the instrument continually scans vertically across the target, and both the Sun and Moon subtend 32 arcminutes, the transmission at each tangent altitude is measured many times during an event. In addition, by measuring the unattenuated target (along LOS's which do not intersect the Earth's atmosphere) the instrument is recalibrated during each event. Therefore, the instrument provides not only accurate, high vertical resolution measurements of atmospheric transmission, but measurements which are relatively immune to drift in instrument performance.

Figure 3.1.2 illustrates the operation of the SAGE III instrument during a typical sunrise event. The two solid lines in the figure represent the upper and lower edges of the Sun as viewed from the spacecraft during the course of the event. The apparent narrowing of the solar image in the lower atmosphere is the result of refraction. The "saw-tooth" line represents the relative motion of the instrument mirror as it scans across the Sun at a nominal rate of 15 arcminutes s^{-1} . As soon as the instrument acquires the Sun in the lower atmosphere, the initiation of a sunrise event, the IFOV is centered long the radiometric center of the solar image and the scan mirror will move up and down to provide vertical scanning of a solar disk. The scanning motion continues until the tangent altitude reaches

300 km. Figure 3.1.3 shows an example of the measured radiance (expressed in counts) for a SAM II 1000 nm event. The scans are alternately upscans and downscans following solar acquisition. Note the peak intensity of each scan gradually increases until it is constant after approximately 40 s, indicating that the Sun is above the atmosphere. In this example, the attenuation in the lower atmosphere is dominated by Rayleigh and aerosol scattering.

The occultation technique is rather unique in that the measurement coverage, both spatial and temporal, is strongly linked to the orbit parameters of the spacecraft. With one of the prime scientific objectives being the determination and monitoring of trends in atmospheric constituents, SAGE III must be deployed in a fashion which yields adequate spatial (latitudinal) and temporal (seasonal) coverage. The current planned implementation for SAGE III is to place one instrument in a sun-synchronous orbit and another, concurrently, in a mid-inclination orbit. The addition of a second occultation target, the Moon, increases the sampling and offers complementary coverage, for example, the ability to make measurements during the polar winter night where sunrises and sunsets do not occur.

The spectral variation of atmospheric extinction is illustrated in Figure 3.1.4 showing the contribution of atmospheric extinction versus wavelength from the different constituents at an altitude of 18 km. Both aerosol and Rayleigh scattering contribute at all wavelengths. Ozone has strong absorption in the Hartley-Huggins band (UV) and the Chappuis band in the visible. NO_2 absorbs between 350 and 600 nm. Water vapor has absorption lines throughout the visible, but with a strong band near 940 nm. NO_3 has absorption features between 500 and 650 nm, and OCIO has a strong band at 350 nm. SAGE III utilizes the spectrometer with the CCD detector to provide spectral measurements over the wavelength ranges from 280 to 1040 nm so that all of these gaseous species can be detected. An additional channel at 1550 nm is used for near IR aerosol extinction measurements. While SAGE III makes 809 individual spectral measurements, in practice only 70-80 discrete values (combinations of 1 or more digitized CCD element measurements) will be routinely transmitted to the ground. These are sufficient to retrieve all gaseous species and aerosol parameters.

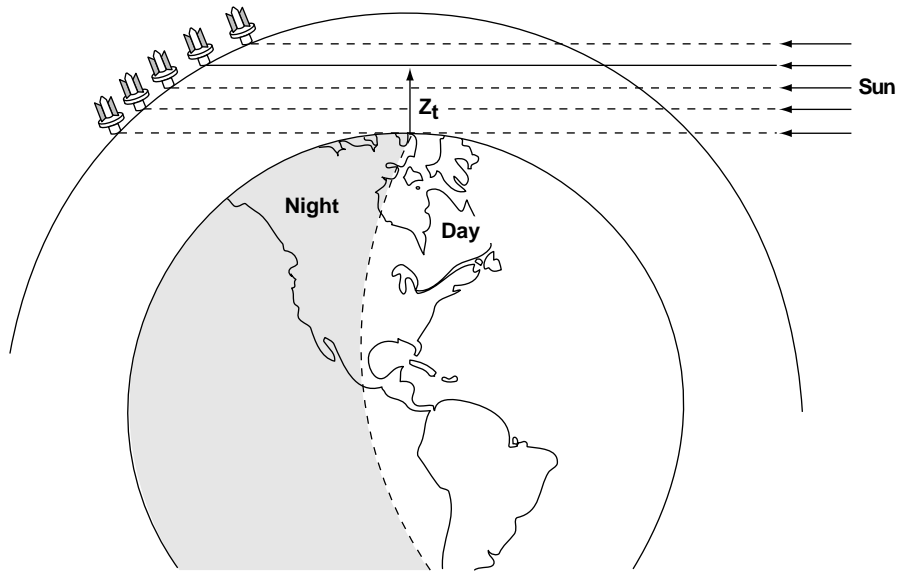


Figure 3.1.1 SAGE III solar occultation measurement geometry. The tangent altitude is denoted by Z_t .

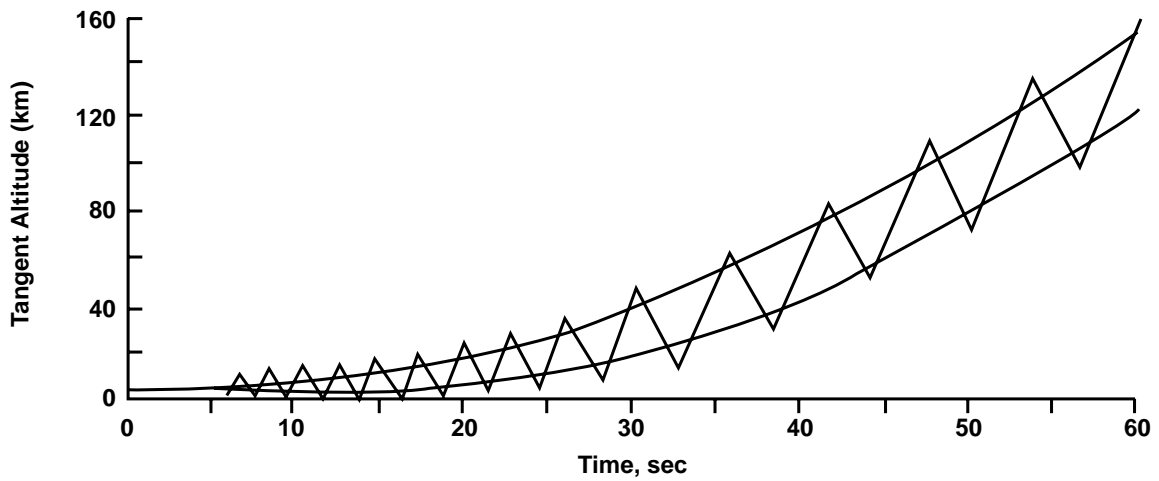


Figure 3.1.2 Typical sunrise event: lines indicate position of top and bottom of the Sun, and scan motion of SAGE III scan mirror across the solar disk.

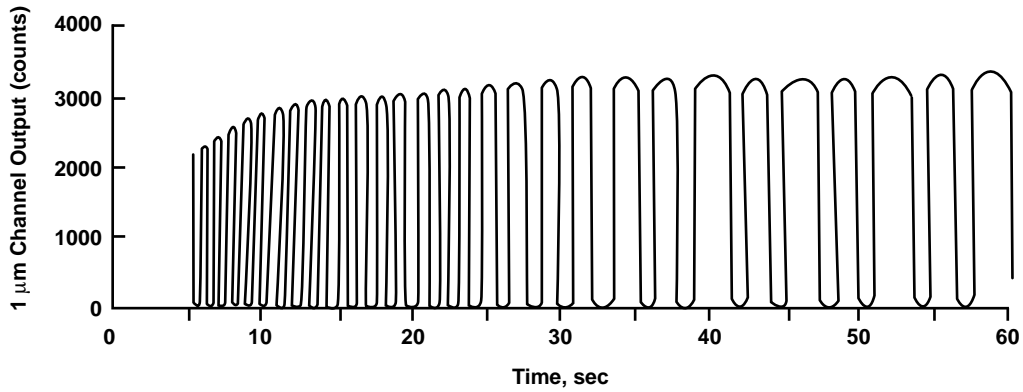


Figure 3.1.3 An example of 1000 nm extinction from SAM II during a sunrise event.

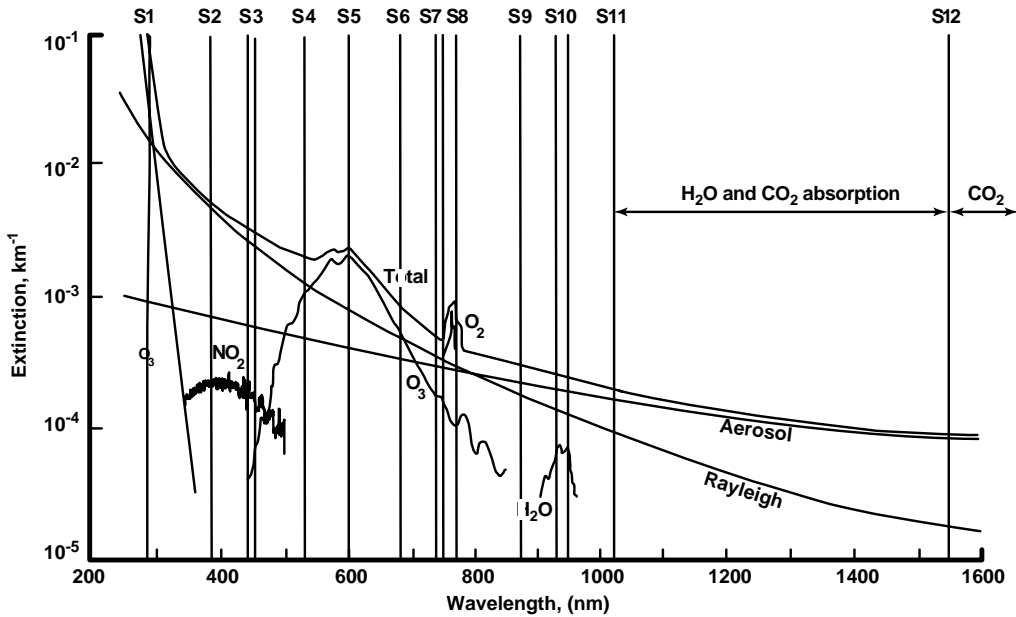


Figure 3.1.4 Wavelength dependence of atmospheric extinction at 18 km (NO_3 and OCIO are not shown).

3.1.2 The Forward Problem

The equation of radiative transfer in one dimension for radiance, $I(\lambda, x)$, at wavelength λ , at an arbitrary point x is given by

$$\frac{dI(\lambda, x)}{d\tau(\lambda, x)} = S(\lambda, x) - I(\lambda, x), \quad (3.1.1)$$

where S is the source function and $d\tau(\lambda, x)$ is the optical depth between points x and $x+dx$. The optical depth per unit distance ($d\tau(\lambda, x)/dx$) is commonly referred to as extinction. The source function consists of contributions from both single and multiple

scattering as well as emission. For SAGE III measurements, wavelengths, and geometry (directly observing the Sun through a small IFOV), scattering and emission terms are very small relative to the directly transmitted component and can be ignored. Therefore, Equation (3.1.1) can be simplified to

$$\frac{dI(\lambda, x)}{d\tau(\lambda, x)} = -I(\lambda, x). \quad (3.1.2)$$

The solution to this equation, when the unattenuated radiance (at $x=0$) is given by $I(\lambda, 0)$, is given by

$$I(\lambda, x) = I(\lambda, 0)e^{-\tau(\lambda, x)}. \quad (3.1.3)$$

Then, the irradiance, R_N as measured by SAGE III for channel “ N ”, can be expressed as

$$R_N(Z_t) = \int_{\Delta\lambda} d\lambda \int_{\Delta\Omega} d\Omega I(\lambda, 0) e^{-\tau(\lambda, Z_t)} W(\Omega) \Psi(\lambda), \quad (3.1.4)$$

where $\tau(\lambda, Z_t)$ is the optical depth along the line of sight at tangent height Z_t between the instrument and the Sun, $\Delta\lambda$ is the spectral width of channel N with band pass function $\Psi(\lambda)$, $\Delta\Omega$ is the angular field of view of the instrument with response $W(\Omega)$. The value of $\tau(\lambda, Z_t)$ varies with tangent altitude; it is effectively 0 above 100 km and generally increases downward. It is composed of contributions from Rayleigh, aerosol, and gaseous species extinction. Transmission along the line of sight, $T_N(Z_t)$ (also called the slant path transmission), at tangent height Z_t , is defined as

$$T_N(Z_t) = R_N(Z_t) / R_N(Z_t^*), \quad (3.1.5)$$

where (Z_t^*) is a tangent altitude well above the atmosphere (> 100 km).

3.2 Retrieval Algorithm Description

3.2.1 Overview and Assumptions

The SAGE III retrieval algorithm is the procedure that converts measured radiances at 70 to 80 wavelengths between 290 and 1550 nm into vertical profiles of the molecular density of gaseous species, aerosol extinction at 8 wavelengths, temperature, and pressure. This procedure consists of two main parts: the transmission algorithm and the inversion algorithm. The different steps in the transmission and inversion algorithms and the overall flow of the algorithm are illustrated in Figure 3.2.1. A brief overview of the different components of the algorithm is provided here so that the readers will have a general understanding of the approach planned for the processing of the SAGE III measurements.

The function of the transmission algorithm is to produce multi-wavelength slant path transmission profiles from time sequences of radiometric and engineering measurements by the SAGE III instrument. As shown in Figure 3.2.1, this process can be separated into five components: data screening, position registration, wavelength registration, radiance calibration, and data grouping and statistics. The first step in the transmission algorithm is the screening of the input level zero (telemetry) data. The data screening algorithm will locate missing or bad data and determine whether the data are recoverable. Next, the position registration algorithm determines where the instrument is looking during a measurement in terms of position on the solar disk and tangent height in the Earth's atmosphere for the line-of-sight that originates from the center of the instrument's field view to the designated position on the Sun. The solar limb position information is necessary for ratioing the atmospheric Sun scan data to the exoatmospheric Sun scan data to generate atmospheric transmission values, while the tangent height information is necessary to provide height registration of the derived transmission values in the atmosphere. A correction for atmospheric refraction is applied to the position registration for tangent altitudes in the lower atmosphere (below approximately 25 km). The next step is the wavelength registration in which the solar spectra measured by the SAGE III CCD spectrometer system are fitted to match well known solar spectra including Fraunhofer lines. In this manner, shifting and stretching of the pixels on the CCD device due to thermal or mechanical perturbations can be accounted for and the center wavelength for each of the 809 pixels will be accurately determined. It should be noted that the instrument spectral sampling does not meet the Nyquist criteria and that the algorithms have been developed so as not to alter or interpolate the measured data in any way. Wherever it is required, external data (such as absorption spectra) are placed on the measurement wavelength grid and these data do meet the Nyquist criteria. The radiance calibration algorithm is the step that actually produces the multi-wavelength slant path transmission profiles by ratioing the atmospheric Sun scan data to the exoatmospheric Sun scan data. The final step in the transmission algorithm is the data grouping and statistics. This procedure groups derived transmittance data (up to several thousand scans per wavelength) into a more manageable size and performs a statistical analysis to determine the characteristics of the distribution of the measured data in each group. A random uncertainty estimate is generated to indicate the quality of the measurements in each group. The final output of the transmission algorithm are profiles of multi-wavelength slant path transmission data with associated uncertainty estimates.

The inversion algorithm converts the multi-wavelength slant path transmission data from the transmission algorithm into vertical profiles of molecular density for SAGE III measured gas species, aerosol extinction at 8 wavelengths, and atmospheric temperature and pressure. The individual steps in this inversion process (shown in lower half of Figure 3.2.1 actually work with slant path optical depth instead of transmission. The slant path optical depth at each of the SAGE III measurement wavelengths has contributions from Rayleigh scattering, aerosol extinction, and absorption from typically one or more gaseous species. These components must be determined before the retrievals of the individual constituents can be performed. Rayleigh scattering contributes to the optical depth at all wavelengths but can be accurately estimated from the atmospheric temperature and pressure. On the initial iteration, the Rayleigh component is estimated

from the first guess temperature and pressure profiles provided by the National Centers for Environmental Prediction (NCEP). On subsequent iterations, the Rayleigh component is estimated from the temperature and pressure profiles derived internally using the SAGE III oxygen A-band measurements. The next step is to derive slant path optical depths for NO₂ and O₃ over the spectral region from 400 to 650 nm using a multiple linear regression (MLR) technique (discussed in detail in Section 3.2.3 of the SAGE III Solar and Lunar Algorithm ATBD). The advantage of the MLR technique is that the fine structure of NO₂ and O₃ in this spectral region allows the determination of the column densities without knowledge of the aerosol or molecular components. Additionally, the 450 nm aerosol optical depth will be determined at this point from the residuals of the MLR. The next step in the inversion algorithm is the separation of the aerosol and O₃ components for the Chappuis band channels and the aerosol channels at 525, 670, 757, 872, 1020, and 1550 nm using a least squares technique. Once this stage has been completed, the algorithm proceeds with the retrieval of the water vapor molecular density profile from the slant path optical depth measurements in the 940 nm spectral region. A global fitting technique is used for the water vapor retrieval because it is the only absorber that exhibits any significant spectral variability over this region and that variability is superimposed on a relatively smooth aerosol and Rayleigh background. The next step in the inversion algorithm is the retrieval of temperature and pressure (T/p) profiles from the SAGE III measurements of the oxygen A-band transmission in the 760 nm spectral region. The temperature and pressure retrievals are difficult due to the nonlinearity of the problem and use a global fitting approach based on the Marquardt nonlinear least squares algorithm. The retrieved temperature and pressure profiles replace the current working T/p profiles (initially provided by the NCEP). At this point in the inversion algorithm, a convergence test is performed on the retrieved temperature and pressure profiles (see Section 3.2.2 for details). If the convergence criteria are met, then the inversion algorithm proceeds to the final stage which consists of retrieving aerosol extinction at 385 nm and the reduction of the slant path column O₃ and NO₂ molecular densities and aerosol slant path optical depth at 8 wavelengths to vertical profiles of either molecular number densities or aerosol extinction. At this point all species have been transformed to vertical profiles and the construction of the data products listed in Table 1.5.1 is performed.

SAGE III estimates of gas species are expressly dependent on the quality of spectroscopic data for both primary and interfering species. An assessment of the current state of relevant spectroscopic data is given in Appendix C. The SAGE III retrieval algorithm also assumes that the atmosphere is horizontally homogeneous on scales of at least 200 km. While this is generally applicable to the stratosphere, this assumption is not always valid. For instance, diurnally varying gases such as NO₂ and O₃ (in the mesosphere) may exhibit a gradient across the terminator. In these cases, both a profile and the slant path concentrations as a function of tangent height will be standard data products (see Table 1.5.1). A more difficult problem is observations of clouds either in the troposphere or in the polar stratosphere. By experience with SAGE II, it is known that both types of cloud are not generally homogeneous and may have a deleterious effect on the estimates of gas species molecular concentration as well as aerosol extinction. This issue is discussed in more detail in the clouds data products ATBD.

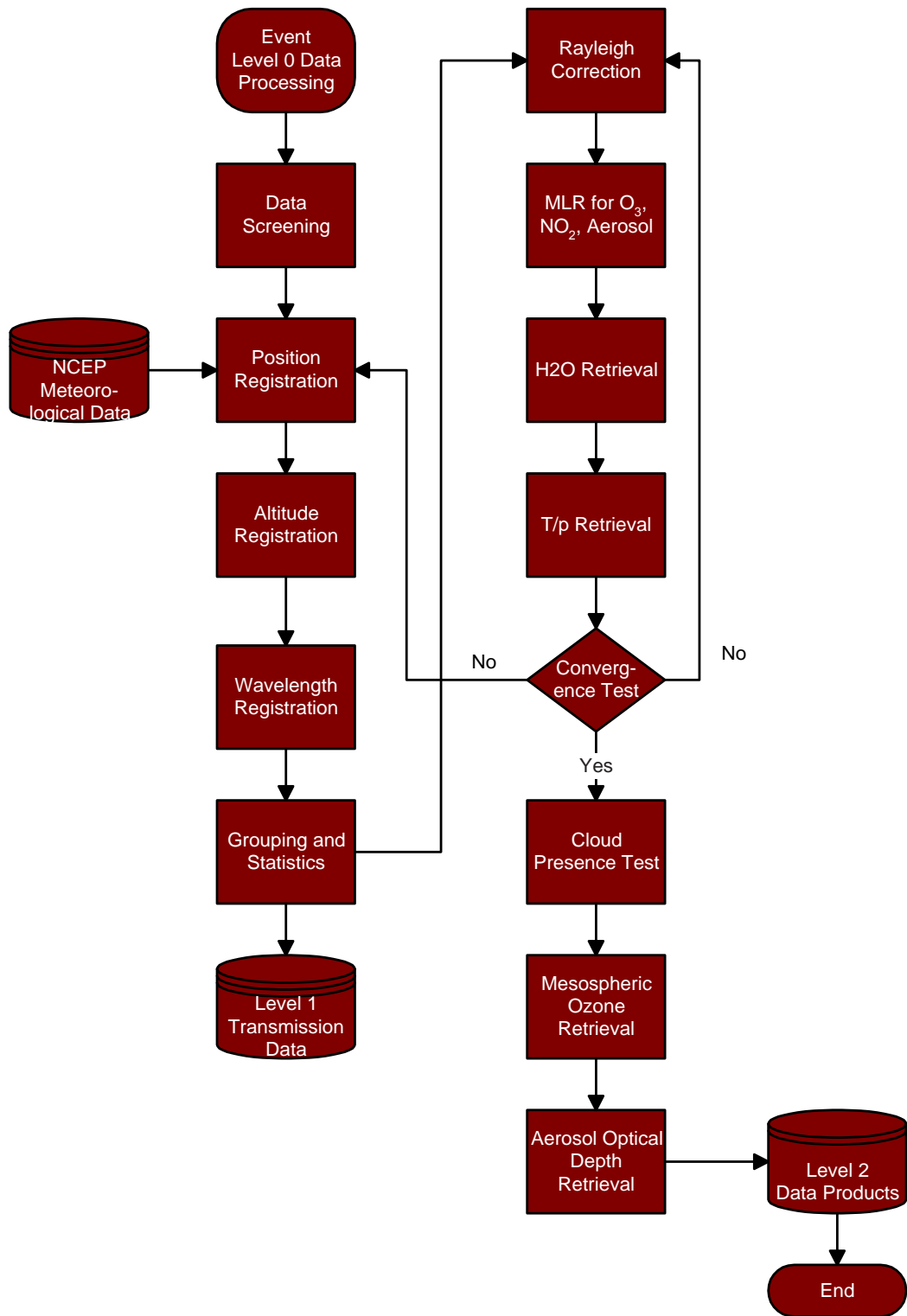


Figure 3.2.1 Flow of data through the SAGE III processing algorithm.

3.2.2 Algorithm Mathematical Description

For the SAGE III measurement geometry, Equation (3.1.4) can be rewritten for the irradiance $R(t, \lambda)$ as a function of time as measured by the SAGE III instrument as

$$R(t, \lambda) = \int_{\Delta\lambda} \int_{\Delta\Omega} W(\lambda', \theta, \phi, \lambda) \Psi(\lambda') S(\lambda', \theta, \phi, t) T(\lambda', \theta, Z_t) d\Omega d\lambda' \quad (3.2.1)$$

where W is the instrument field of view function, ϕ is the azimuthal angle, θ is the elevation angle, Ω the instrument solid angle, Ψ is the optical filter bandpass function, S is the extraterrestrial solar radiance, and T is the atmospheric slant path transmission as a function of the viewing angle θ or tangent height Z_t .

For the data acquisition geometry utilized by SAGE III where the elevation mirror vertically scan across the solar limb, there is a one-to-one relationship between the elevation angle $\theta(t)$ to the tangent height of the line-of-sight Z_t . Similarly, with the Sun in the field-of-view, the elevation angle $\theta(t)$ at a specific time will be pointing to a unique value of the solar limb position p . p is defined from the suntop in angular unit along the elevation direction. Substituting Z_t and p as the dependent variables for the irradiance measurements R , we can write $R(p, Z_t, \lambda) = R(\lambda, t)$.

For an instrument such as SAGE III with small instantaneous field-of-view (IFOV) and where the solar limb profiles are slow varying, Equation (3.1.4) can be approximated by

$$R(p, Z_t, \lambda) = \int_{\Delta\lambda} \Psi(\lambda') \bar{S}(p, \lambda') \bar{T}(Z_t, \lambda') d\lambda' \quad (3.2.2)$$

Where the over-bar denotes the average value over the field-of-view, i.e., $\bar{S}(p, \lambda)$ is the mean value of $S(p, \lambda)$ center at p , and

$$\bar{T}(Z_t, \lambda) = \int_{\Delta\Omega} W(\theta, \phi, \lambda) T(\theta, \lambda) d\Omega \quad (3.2.3)$$

is the mean slant-path transmission profile integrated over the instrument's instantaneous field-of-view W . For the solar limb profile with slow variation with wavelength, we can further simplify the Equation (3.2.2) to

$$R(p, Z_t, \lambda) = \bar{S}_\lambda(p) \langle \bar{T}(Z_t, \lambda) \rangle \quad (3.2.4)$$

where the bracket denotes integrated value over the wavelength filter function, and $\bar{S}_\lambda(p)$ is the mean value of S at λ . So that

$$\langle \bar{T}(Z_t, \lambda) \rangle = \int_{\Delta\lambda} \Psi(\lambda') \bar{T}(Z_t, \lambda') d\lambda' \quad (3.2.5)$$

For high altitude where Z_t becomes Z_t^* , normally greater than 100 km height, we have $\langle \bar{T} \rangle$ approaching unity with no significant absorption or scattering in the atmosphere, therefore we have

$$R(p, Z_t^*, \lambda) = \bar{S}_\lambda(p) \quad (3.2.6)$$

and the mean transmission can be expressed as

$$\langle \bar{T}(Z_t, \lambda) \rangle = R(p, Z_t, \lambda) / \bar{S}_\lambda(p) = R(p, Z_t, \lambda) / R(p, Z_t^*, \lambda) \quad (3.2.7)$$

Equation (3.2.7) illustrates the basic approach for the transmission algorithm, where a mean transmittance can be obtained from the ratio between solar irradiance measurements inside and outside the atmosphere. Notice that

$$R(\lambda, t) = G_\lambda L_\lambda(t) \quad (3.2.8)$$

where G_λ is the instrument throughput gain function for wavelength λ and $L_\lambda(t)$ is the channel digital count data. Substituting Equation (3.2.8) into Equation (3.2.7) we obtain,

$$\langle \bar{T}(Z_t, \lambda) \rangle = L(p, Z_t, \lambda) / L(p, Z_t^*, \lambda) \quad (3.2.9)$$

The instrument response function G_λ cancels out and the mean transmittance only depends on the ratio between the two measured digital count values. Equation (3.2.9) is the basic for claiming that SAGE III measurements are self-calibrated and are not susceptible to long-term instrument degradation.

The mean transmittance as a function of atmospheric parameters is given by

$$\langle \bar{T}_\lambda(Z_t) \rangle = \exp[-\tau(\lambda, Z_t)] = \exp[-\int \beta(\lambda, Z_t) dl(\lambda, Z_t)] \quad (3.2.10)$$

where $\tau(\lambda, Z_t)$ is the total slant path optical depth, $\beta(\lambda, Z_t)$ is the total extinction coefficient, and $l(\lambda, Z_t)$ is the geometrical slant path corrected for refraction [Chu, 1983]. The total extinction is a linear combination of the extinctions due to each of the component species in the atmosphere:

$$\beta(\lambda) = \beta_{Rayleigh}(\lambda) + \beta_{O_3}(\lambda) + \beta_{NO_2}(\lambda) + \beta_{aerosol}(\lambda) + \beta_{othergases}(\lambda) \quad (3.2.11)$$

where the extinction due to gaseous species is given by the integral along the optical path through the atmosphere

$$\beta_{gas}(\lambda) = \sum K(\lambda, k, p) \rho \quad (3.2.12)$$

where $K(\lambda, k, p)$ is the absorption cross section, ρ is the species number density, k in this case is the temperature, and p is the pressure. The aerosol extinction, with the assumption of homogeneous, spherical particles, may be obtained from Mie theory as

$$\beta_{aerosol}(\lambda) = \int_0^{\infty} Q(n, r, \lambda) N(r) dr. \quad (3.2.13)$$

These equations describe completely the relationship between the attenuation property of the atmosphere to the measured radiance at a specific geometry defining the position of the spacecraft, the target (Sun / Moon), and the Earth.

The main purpose of the algorithm being described here is to convert the time registered radiance data into atmospheric transmittance associated with each measured solar radiance at the given tangent height level in the atmosphere. The conversion process will involve accurately positioning the measured data point on the Sun and in the atmosphere, and then performing a ratio to a well calibrated solar limb curve [Chu and McCormick, 1979]. The inversion procedure for retrieving the vertical profiles for the different species from the transmission data for SAGE II is discussed in the literature [Chu *et al.*, 1989; Chu *et al.*, 1993]. The algorithm for the SAGE III measurements is discussed in the different documents (see section 1.3).

3.2.3 Algorithm Description

The transmission data product algorithm as discussed here can be separated into five main functions: Data screening, position registration, wavelength registration, radiance calibration, and data grouping and statistics. A complete flow-chart diagram showing the data flow for the SAGE III level 1B production algorithm is illustrated in Figure 3.2.1 In the following, detailed descriptions of the processes involved in the flowchart diagram are given below.

Data Screening

The data screening for the transmission algorithm consists of three parts. The first part deals with data calibration, the second part deals with input level 0 data screening, and the third part deals with data screening after the radiance data have been calibrated in position.

Data Calibration

The data calibration for the SAGE III measurements consists of calibration of detector dark current, linearity of detector response, and change of scan mirror reflectivity with varying incident angle. The SAGE III instrument will perform these calibration activities approximately once a day, and the analysis of the calibration data will be done on a weekly basis to update the instrument calibration data file. These updated calibration data files will then be used by the operational algorithm to process the SAGE III telemetry data.

For detector dark current calibration, the instrument will be power-on over the dark side of the orbit with the attenuation filter over the telescope. With the sensor pointing at dark space, background dark current from each pixel will be measured at selected integration times.

Linearity calibration of the detector response will be performed using the dark current as the signal source. By varying the integration time of the detector so that the integrated dark current signal levels will cover the dynamic range of the detector response, the departure from linearity of the detector response can be calculated from the calibration data. Laboratory linearity test on the SAGE III CCD detector using this approach has shown that the departure from linearity for the flight-type detector is below 0.03 % of the full scale response of the instrument.

Since the scan mirror will be operated near the Brewster angle for most of the atmospheric measurement, polarization effect will produce changes in the total reflectivity of the scan mirror as a function of incident angle. This problem has been an inherent problem for the SAGE series of instruments, and a calibration methodology has been developed to correct the measured signal. Exoatmospheric sun scan data will be taken from about 300 km to 100 km tangent height during a mirror calibration event.

These data will be analyzed to produce a reflectivity versus angle correction curve for each of the radiometric channel on SAGE III. This curve will be extrapolated to the angular range where atmospheric data are being taken (from 100 km down to sea level tangent height). This calibration procedure has been verified to be very accuracy for the SAGE II instrument.

The above discussed calibration data will be used to correct the level 0 data during the input data screening procedure as discussed in the following.

Input Data Screening

The data screening for the SAGE III level 0 data ingest is performed prior to any analyses of the raw radiance data. The data screening algorithm is tailored to the SAGE III processing algorithm in term of handling missing raw radiance data. Since the level zero processing will only provide indication of erroneous data in the data packet, the algorithm here will locate the bad data, check for whether the data are recoverable. If the problem is due to bit hit, then it is possible to recover by doing interpolation or other procedure. If the bad data have corrupted the whole Sun scan, then the algorithm will determine whether the whole scan can be recovered. If the radiance data in the particular scan cannot be recovered, then the complete scan will be eliminated from the input data stream.

Calibrated Data Screening

Additional screening of the radiance data will be accomplished after the position registration process has been completed for each data point. There are two other data screening procedures for the SAGE III calibrated radiance data. The first screening is

applied to the sun-scan data which are contaminated by sunspots. Sunspots can easily be identified from the solar limb curve at near IR wavelengths. They normally exhibit as sharp drop in intensity over an angular region about a few arc-minutes. Sunspot signature can easily be identified by comparing the measured solar limb curve to a standard solar limb curve. This procedure is effective when the measurements are sufficiently high in the atmosphere, above 50 km in altitude where negligible atmospheric attenuation will occur. Lower in the atmosphere, it would become difficult to separate between sunspot and cloud signatures. As soon as the sunspot has been identified, the location of the sunspot on the solar limb position will be flagged so that no radiance data measured at those positions will be used for the determination of atmospheric transmission. The second screening process is related to eliminating the data points outside the solar limb curves. Since the scan mirror will scan past the Sun edge before turn around, a fraction of the scan data will be taken when the field-of-view is off the solar disk. These data points will be analyzed for background noise level before being eliminated for future processing.

The sunspot screening procedure will also be able to discriminate between Sun spots that have been rotated into the instrument scan direction, and the occurrence of polar mesospheric clouds (PMC's). The rotation of the Sunspots into the instrument's field-of-view occurs because of the orbital geometry between the Sun and the spacecraft where the image of the Sun can rotate on the image plane of the instrument during a measurement event. Sun scans will be monitored at all altitudes above cloud top for the occurrence of Sunspots. Sunspots can be identified from the signature occurring at the same solar limb position during consecutive scans. The PMC signatures will look like Sunspots except that they occur at the same altitude in the atmosphere. This is the criterion for the separation between sunspot and PMC signatures.

Position Registration

As indicated by Equation (3.2.9), to convert the radiometric measurements into atmospheric transmittance, we need to specify the location information for each datum. Basically there are two positions that need to be determined accurately for each measurement. The first is the position on the solar limb p in angular unit, and the second is the tangent height Z_t in the Earth's atmosphere for the line-of-sight that originates from the center of the instrument's field-of-view to the designated position on the Sun. The first position information is used for rationing the within atmospheric Sun scan data to the exoatmosphere Sun scan data to generate atmospheric transmission values, as indicated by Equation (3.2.9), while the second position information is used to height-register the derived transmission values in the atmosphere, as indicated by Equation (3.2.10). The determination of the measurement position on the Sun is complicated by the scanning motion of the field-of-view of the instrument. For example, one can determine accurately the spacecraft to Sun / Moon and Earth geometry at each instance of time by performing a detailed ephemeris calculation. However, the calculation only provides the geometry for the Sun at either the Sun top, Sun bottom, and the Sun center, while the instrument's field-of-view is somewhere within the solar limb. Therefore one has to include the scanning motion of the scan mirror in order to determine the exact position of

the field-of-view with respect to some reference point on the Sun at each instance of time. In this algorithm, the reference point on the Sun is the Sun top since a well defined Sun edge signature can be determined there.

Spacecraft / Instrument to Sun / Moon and to Earth Geometry

For a given SAGE III measurement at time t , where the time can be converted to universal time, one can accurately determine the spacecraft relative to the Sun/Moon and the Earth geometry using both the spacecraft and the Sun / Moon ephemeris data. The computation of the spacecraft ephemeris relative to the Earth / Sun geometry can be done using simple approximation calculation or with fully complex calculation as described in the various references. [Buglia; 1988, 1989]

Base on the experience with the processing of previous SAGE and SAGE II experiments, the computational scheme as developed by Buglia has been found to be sufficiently accurate for processing the SAGE measurements. Buglia's computational method is based on the propagation of the state vector of the spacecraft at time t to $t + \delta t$ using Kepler Second Law. The propagation time is limit to well within one minute to guarantee the accuracy of the extrapolation. The computational result will provide the elevation angle of the line of sight from the spacecraft/instrument to the top of the Sun, together with the tangent height of the line-of-sight to the sea level point with latitude and longitude information. The complete geometry is calculated with this algorithm without the atmospheric refraction correction. Correction with atmospheric refraction is discussed in the next section.

Atmospheric Refraction Correction

As is indicated in Figure 3.1.1 and discussed in section 3.2.2, atmospheric refraction becomes important for measurements with tangent altitudes below 25 km. In principle, most measurement positions can be determined with straight line light ray propagation from the Sun through the Earth's atmosphere to the SAGE III instrument. However, in the lower atmosphere, typically below 25 km altitude, light rays will be bent due to the varying atmospheric density gradient, resulting in a curved trajectory for the light ray. Therefore the determination of image position for the SAGE III measurements will be changed from a straight line geometrical calculation to a methodology that is capable of handling the bending of the ray path. Various methods used for the calculation of atmospheric refraction effect have appeared in the published literature over the last few decades. One of the methodology that was developed by Chu [1983] has been successfully applied to the data processing for the SAGE series of spaceborne occultation measurements. Chu's method utilizes the expansion of the refraction integral in power of the refractivity index value at the ray tangent point to calculate the total bending angle. He was able to derive analytical solutions for the integrals under the condition that the temperature profile can be constructed from linear segments given the temperature values at discrete altitude levels. Comparison of the computational results derived from the analytical solution to those generated from a ray trace calculation showed similar accuracy. The atmospheric refraction calculation provides the total bending angles as a

function of tangent height of the limb viewing ray path. This information can be combined with the spacecraft orbital geometry information to produce the required correction for position determination for the Solar and Lunar measurements.

SAGE III refraction is calculated using the method of Aver and Standish [1972].

Instrument Scanning Geometry

The scan pattern over the solar disk as illustrated in Figure 3.1.2 will provide the SAGE III instrument with measurements across the solar limb where the calibration of the data can be done easily due to the stability of the solar limb radiance profiles. To determine the position of each measurement on the solar limb and also the corresponding height in the atmosphere, the scanning pattern or motion of the SAGE III instrument has to be included in the analysis. Consider a down scan where the instrument's field-of-view moves from a high point above the solar disk onto the Sun, crossing the top sun-edge at t_1 , and continuing until time t_2 where the instrument's field-of-view is some where on the solar limb. Since the scanning motion of the SAGE III instrument moves 15 arc-minute per second while the solar image also move across the image plane vertically with an angular rate approximately 3 arc-minute per second (depending on orbit height), the effective rate of scanning across the solar disk will be an arithmetic sum or difference of the three rates depending on whether it is a sunrise or sunset event where the solar disk moves against or together with the instrument scan direction. The solar limb position can then be directly determined using the effective scan rate and the total time difference between t_2 and t_1 . As far as determining the tangent height location in the atmosphere, the instrument scan rate and the time interval between t_2 and t_1 will be used to determine the net angular distance traveled from the sun-top angular position to the angular position at t_2 . These angles can be directly converted to tangent altitude from the measurement geometry. For lower atmospheric scan where atmospheric refraction effect becomes importance, the atmospheric correction analysis as discussed above can be used to adjust the results obtained from the procedure described in this section. To determine the position registration problem for an up scan will be similar with the procedure described above. In this case the top edge of the solar disk will still be used as the reference point while the scan direction is upward approaching the top edge of the solar disk. The reason that the top edge of the Sun will be used as the reference point for both the up and down scans is that the bottom edge of the solar disk will be the first to be contaminated by clouds and other attenuation during an occultation event.

Scan Data Processing for Refining Position Registration

The procedure for position registration of the SAGE III measurements as described above will produce a position calibrated SAGE III data set. However, with the uncertainty associated with several parameters such as instrument scan rate, Sun edge timing, refraction and other atmospheric effects that are used in the procedures, the position determination results could contain significant uncertainty. A refinement of the position calibration process has been developed that can significantly improve the accuracy of the

position registration results. In the following, a detailed discussion of the refinement procedure is included.

Each solar scan intensity measurement can be expressed as $I(p, z)$ where p is the solar limb position while z is the atmospheric height. The measured $I(p, z)$ can be written as

$$I(p, z) = I_0(p)T(z) + \varepsilon \quad (3.2.14)$$

where $I_0(p)$ is the unattenuated solar limb curve, $T(z)$ is the atmospheric transmission for the slant path geometry, and ε is the error in the measurements. In reality, the above equation can be written as

$$I(p + \varepsilon_p, z) = I_0(p)T(z) + \varepsilon \quad (3.2.15)$$

where ε_p is related to errors in the Sun edge time. There are two cases that can be considered separately. The first case is for measurements high in the atmosphere where $T(z) = 1$, and we can expand the above equation into

$$I = I_0 + a \frac{dI_0}{dp} + bp \frac{dI_0}{dp} \quad (3.2.16)$$

where the first term I_0 is the estimate for the limb profile, the a term is the linear shift term, and the b term is the linear stretch term. The a and b can be solved for using the Multiple Linear regression (MLR) (Bevington, 1966: see SAGE III Solar and Lunar ATBD) technique by calculating the $\frac{dI}{dp}$ terms using finite difference. These a 's and b 's along with the scan rate information are then used to evaluate the ε'_i 's which are the edge time corrections.

The second case involves scan measurements in the atmosphere where $T(z)$ is variable with z . Defining q so that

$$\begin{aligned} I &= I_0 T + \varepsilon \\ &= q + \varepsilon \end{aligned} \quad (3.2.17)$$

with $q = I_0 T$; the uncertainty in p implies that q is unknown, but can be estimated from

$$q = q_0 + a \frac{dq_0}{dp} \frac{dp}{dt} + bp \frac{dq_0}{dp} \frac{dp}{dt} \quad (3.2.18)$$

The $\frac{dp}{dt}$ term accounts for the nonlinear scan across the solar disk due to refraction. Again the expansion terms are the linear shift and stretch terms. Substituting

$$\begin{aligned}
I &= q + \varepsilon \\
&= q_0 + a \frac{dq_0}{dp} \frac{dp}{dt} + bp \frac{dq_0}{dp} \frac{dp}{dt} + \varepsilon
\end{aligned} \tag{3.2.19}$$

Dividing by q_0 we get

$$\begin{aligned}
\frac{I}{q_0} &= 1 + \frac{a}{q_0} \frac{dq_0}{dp} \frac{dp}{dt} + \frac{bp}{q_0} \frac{dq_0}{dp} \frac{dp}{dt} + \varepsilon' \\
&= 1 + a \frac{d \ln q_0}{dp} \frac{dp}{dt} + bp \frac{d \ln q_0}{dp} \frac{dp}{dt} + \varepsilon'
\end{aligned} \tag{3.2.20}$$

in which the coefficients a 's and b 's can be solved from MLR technique to correct for the errors in edge times.

Wavelength Registration

During SAGE III instrument wavelength calibration mode, the instrument will scan across the solar disk at the same nominal scan rate. However, the CCD data will be collected at the 809 pixels and shipped out at a rate of 6 Hz, while the 1550 nm channel data will still be sampled at 64 Hz sampling rate. The 809 CCD pixels readout on the solar limb will then be used for wavelength calibration of the CCD.

The solar spectrum contains several dark line structures, especially pronounced in the shorter wavelength region below 500 nm. Those dark and narrow lines are the solar Fraunhofer lines caused by atomic species absorption in the solar atmosphere. These well-defined solar Fraunhofer lines are used by the SAGE III instrument to perform wavelength calibration of the SAGE III spectrometer, and the CCD pixels. The basic approach here is to fit the CCD response to the well-known solar spectrum, with allowance for shifting and stretching of the pixel locations due to thermal or mechanical perturbation. As a result, we can denote the center wavelength for each of the 809 pixels on the CCD device. The Multiple Linear Regression (MLR) technique discussed in the previous section can be used to perform the wavelength calibration of the SAGE III CCD spectrometer system by fitting the known solar spectra against the measured spectra from the instrument.

Consider $S(x)$ as the measured solar wavelength spectra from the SAGE III CCD spectrometer as a function of the pixel position x . We can assume small displacements from the regular equal spacing of the CCD pixels by expanding $S(x)$ into small displacement dx as

$$\begin{aligned}
S(x_0 + \delta x) &= S(x_0) + \left[\frac{dS(x)}{dx} \right]_{x=x_0} \delta x + \varepsilon \\
&= S(x_0) + a \frac{dS(x)}{dx} + bx \frac{dS(x)}{dx} + \varepsilon
\end{aligned}
\tag{3.2.21}$$

where the small displacement is considered to consist of shift (the a term) and stretch (the b term) in the first order, and ε is the noise term.

The Multiple Linear Regression technique could be used to solve for the wavelength registration problem. Using Equation (3.2.21) with $S(x)$ as the measured solar spectrum, $S(x_0)$ as the predicted solar spectrum from the CCD, the a term describes the linear shift while the b term describes the stretch. The a and b terms can be estimated by least square minimization of the ε_2 , and then used to mark the pixel on a wavelength scale.

Radiance Calibration

The radiance calibration of the SAGE III measurements consists of two parts. The first part is to determine the solar limb profiles for all the spectral channels. These solar limb profiles are selected from the solar scans high up in the atmosphere so that no atmospheric attenuation will occur. The quality of these profiles will be analyzed by average over different scans and possibly separated into two groups consisting of up-scans and down-scans. An interpolation scheme will be used to produce a continuous solar limb profile for each spectral channel. The second part of the radiance calibration process is to ratio the lower atmospheric scans into the calibrated solar scan for the same spectral channel at the same solar limb location. This procedure will remove the data dependence on the solar parameters, and will result in converting the SAGE III measured data into atmospheric transmittance values at the specific tangent height location. As a result of the radiance calibration process, all the SAGE III scan data that are on the solar limb with altitudes below 120 km tangent height will be converted into atmospheric slant path transmittance data at the different spectral channels.

Data Grouping And Statistics

Since the number of SAGE III derived atmospheric transmittance data from the Sun scan measurements could approach several thousands for each of the spectral channel, some sort of data grouping needs to be performed in order to keep the measured data in a manageable size for further processing into vertical profiles of the different species in the atmosphere. One of the way to group the data, as was done in SAGE II and SAGE data, is to group the measured scan data into altitude bins of equal increment from the lowest altitude (which would be either sea level or cloud top) up to a top altitude where the different species concentrations are too small to be measured by the SAGE III instrument. Statistical analysis are then used to determine the characteristic of the distribution of the measured data in each group. For example, if the distribution is normal, then a mean and variance will be sufficient to represent the grouping distribution. However, if the distribution is not clearly normal with large deviations, then a median

may be used instead of the mean. The advantages of the grouping process are, (1) to reduce the subsequent processing requirement by reducing the size of the data; (2) produce a statistical mean value to represent an average for the group; and (3) generate an error estimate for the average value to indicate the quality of the measurements. The altitude increment used for data grouping will be 0.5 km or smaller.

3.3 Algorithm Testing Requirements

Algorithm testing will be performed both prior to launch and during the lifetime of the instrument using the SAGE III data simulator. The data simulator models both a ray tracing-based model of the atmosphere and accounts for measured and modeled instrument performance. For instance, the instrument model includes the effects of uncertainties in the instrument wavelength-band pass, fields of view, detector response, and spacecraft telemetry. The atmospheric model can include realistic uncertainties in errors in external data sets (e.g., molecular spectroscopy and lunar albedo) and the effects of atmospheric spatial inhomogeneity. The simulator should (and has) helped us to identify software errors and below standard performance in individual retrieval components. The simulator is maintained under configuration control and is considered an adjunct component of the primary operational software.

3.4 Validation Plan

Planning for the validation of all SAGE III data products is covered in the SAGE III Validation Plan (LARC475-00-020). Validation plans are uncertain due to the slip in SAGE III/Meteor-3M launch date and that document will be revised as launch date and available funds available for validation become more certain.

3.5 Quality Control and Diagnostics

Routine processing will generate a series of quality indicators that assess the quality of the data products and the degree to which the processing of each event was completed according to expectation. The details of this process are outlined in The SAGE III Data Management System Quality Assurance Document (LaRC475-03-115).

3.6 Exception Handling

Process exception handling falls into two categories: process failure and process monitoring. In the failure case, the production code is unable to complete processing and null data is generated to indicate the absence of valid data. In the second case, post processing comparisons generate a series of quality assessment indicators that may be screened to isolate unusual data. In no case, if the processing is completed will data be suppressed; rather, the data quality indicators will be used to indicate the degree to which

the intermediate and final products conform to a set of expectations established in the integration and testing process.

4.0 References

- Bevington, P. R., *Data Reduction and Error Analysis For the Physical Science*, McGraw-Hill, N. Y., 1969.
- Buglia, J. J., *Compilation of Methods in orbital mechanics and solar geometry*, NASA RP-1204, 1988.
- Buglia, J. J., *Effects of ephemeris errors on the accuracy of the computation of the tangent point altitude of a solar scanning ray as measured by the SAGE I-II instruments*, NASA TP-2866, 1989.
- Chu, W. P. and M. P. McCormick, Inversion of stratospheric aerosol and gaseous constituents from spacecraft solar extinction data in the 0.38 - 1.0 microns wavelength region, *Appl. Opt.*, 18, 1404, 1979.
- Chu, W. P., M. P. McCormick, J. Lenoble, C. Brogniez, and P. Pruvost, SAGE II inversion algorithm, *J. Geophys. Res.*, 94, 8339, 1989.
- Chu, W. P., E. W. Chiou, J. C. Larsen, L. W. Thomason, D. Rind, J. J. Buglia, S. Oltmans, M. P. McCormick, and L. R. McMaster, Algorithms and sensitivity analyses for SAGE II water vapor retrieval, *J. Geophys. Res.*, 98, 4857, 1993.
- Mauldin, L. E., Stratospheric Aerosol and Gas Experiment II instrument: A functional description, *Opt. Eng.*, 24, 2, 307-312, 1985.
- Mauldin, L. E., M. P. McCormick, J. M. Zawodny, L. r. McMaster, W. P. Chu, J. C. Gustafson, and G. L. Maddrea, The Stratospheric Aerosol and Gas Experiment III Instrument proposed for EOS: a conceptual design, *Int. Congress on Opt. Sci. and Eng.* - Paris, France, 1989.
- McCormick, M. P., P. Hamill, T. J. Pepin, W. P. Chu, T. J. Swissler, and L. R. McMaster, Satellite studies of the stratospheric aerosol, *Bull. Amer. Meteor. Soc.*, 60, 1038, 1979.
- McCormick, M. P., W. P. Chu, G. W. Grams, P. Hamill, B. M. Herman, L. R. McMaster, T. J. Pepin, P. B. russell, H. M. Steel, and T. J. Swissler, High-latitude stratospheric aerosol measured by SAM II satellite system in 1978-1979, *Sciences*, 214, 328, 1981
- McCormick, M. P., SAGE II: an overview, *Adv. Space Res.*, 7, 219, 1987.
- McCormick *et al.*, Stratospheric Aerosol and Gas Experiment III (SAGE III) Aerosol and trace gas measurements from Earth Observing System (EOS), SPIE Paper No. 1491-16, *SPIE Symposium on Aerospace Sensing*, Orlando, Florida, 1991.

McCormick, M. P., J. M. Zawodny, W. P. Chu, J. W. Baer, J. Guy, and A. Ray, Stratospheric Aerosol and Gas Experiment III (SAGE III), SPIE International Symposium for Optical Engineering, Orlando, FL, 1993

Pepin, T. J., M. P. McCormick, W. P. Chu, F. Simon, T. J. Swissler, R. R. Adams, K. H. Crumbly, and W. H. Fuller, Stratospheric Aerosol Measurements, in Apollo-Soyuz Test Project. Summary Science Report, NASA SP 412, 127, 1977.

Appendix A. SAGE III Instrument Description

The design of the SAGE III sensor relies heavily upon the flight proven designs used in the SAM II and SAGE I/II instruments. Specifically, the separate sensor and electronics modules concept from SAGE II is utilized, as are the grommet isolation and contamination door designs. Additionally, the SAGE II pointing system and scan mirror designs are reused, with certain necessary modifications (primarily an attenuator filter) to permit solar and lunar observations with the same detector assembly.

The SAGE III sensor assembly, illustrated in Figure A.1, consists of a sun-tracker, telescope, and grating spectrometer with a CCD detector array; the mass is estimated at 35 kg., a volume of 6000 cm³, with an average power of 60 W and a peak power of 75 W. The two-axis passive sun-tracker, with a scan mirror that scans the instrumental field of view across the solar disk, obtains multiple samples at each altitude, improving the measurement precision. Sunspots are readily detected by scanning, rather than staring at the Sun. A pictorial representation of the scanning pattern as a function of tangent altitude and the corresponding detector output (single wavelength) is illustrated in Figure A.2. The two solid lines denote the position of the top and bottom of the solar disk during a sunrise event as viewed from the spacecraft. The gradual expansion of the vertical sun shape is due to atmospheric refraction. The ordinate denotes the tangent altitude, while the abscissa denotes the event time. During an occultation event, the instrument scans the solar disk as indicated by the dashed line in the figure.

The telescope and spectrometer are illustrated in Figure A.3 and constitute new designs optimized to meet the requirements of lunar occultation measurements. The telescope is a f/4 Dall-Kirkham configured design chosen for its ease of alignment; the speed represents a tradeoff between optimum performance and spectral imaging. The spectrometer is a new design, utilizing a holographic, aberration reduced, grating to provide stigmatic imaging at 440 and 868 nm with 1 nm resolution below 450 nm and 2 nm resolution between 740 and 960 nm. The grating is formed on a spherical substrate with a radius of 152 mm and is imaged through a field flattener and order-sorting filters onto the CCD detector. The grating is utilized in the first positive order with diffraction angles between 8.3 and 17.0 degrees; a ruling of 199 lines per millimeter yields a dispersion of 0.94 to 1.88 nm per pixel in the focal plane (depending on wavelength). Evaluation gratings have been tested and demonstrate near-theoretical first-order efficiencies with very low scattered light properties. The spectrometer has been ray-traced and a Monte Carlo simulation of optical tolerances has been performed which indicates that at the wavelengths of best spectral focus, a FWHM bandpass of less than 1.2 nm per pixel should be achievable.

The detector assembly consists of two elements, a Tektronix 809x10 pixel backside-illuminated, thinned CCD array for the 280 - 1040 nm spectral region and a InGaAs infrared photodiode (1550 ± 15 nm) that are spatially co-registered. The 809 elements of the array provide the spectral information, the 10 pixels aligned along the horizontal direction are summed together and can be considered a single long pixel. Practical

considerations favor pixel subdivision: large pixels can have a low charge transfer efficiency which can be avoided through subdivision, and secondly reducing the horizontal instantaneous field of view (IFOV) can improve the probability of cloud-free measurements. Consequently, in the solar occultation mode, 3 pixels (0.5x1.5 arcminute IFOV) are used to improve the frequency of penetration of the measurements into the troposphere. In contrast, for the lunar occultation measurements, all 10 pixels are used to collect more light.

In the solar occultation mode, the optical throughput of the instrument (grating efficiency and CCD quantum efficiency) combined with the spectral variation in the solar spectrum produce a wide variation in the rate of charge accumulation in the CCD pixels as a function of wavelength. Optimum performance (signal-to-noise ratio and dynamic range) of the detector is achieved when pixels are operated at or near full well. To obtain full well across the spectral region, a spectral flattening filter was considered to selectively attenuate the spectrum near the middle of the spectral band pass, but was determined to be too difficult to design. Instead, the array has been divided into eight segments that have individually controlled integration times to control the filling of the wells. Each segment is operated at or near full well, and the transitions between segments are chosen to avoid potential science channels. This solution optimizes performance and eliminates an item of significant risk and cost.

The lunar occultation measurements are significantly more complicated than the solar measurements; depending upon phase, the Moon is between one million and ten million times less luminous than the Sun, and the lunar albedo is non-uniform making determination of atmospheric transmission non-trivial. The instrument is designed to compensate for this large change in illumination in part by removing the solar attenuator (a neutral density filter with an attenuation of 100) from the optical path. In addition, the integration time is increased from 0.09-2.2 milliseconds to 62 milliseconds (with a resulting increase in signal of 28 to 500), and the instrumental field of view is increased from 3 pixels to 10 pixels (producing an increase of 3.3 in signal level). The resulting gain increase of 165,000 should permit lunar measurements with a signal-to-noise ratio of 150-300, only a factor of 10-20 times poorer than the solar measurements which implies that the altitude range for the species retrievals will be somewhat reduced in the lunar occultation mode.

The detector package has been modeled and electrical, optical, thermal, and radiation-shielding testing of prototype detectors has been performed. The detector assembly is surrounded by an aluminum radiation shield (nominally 1-inch thick) and is illustrated in Figure A.4. The housing is comprised of a base plate, a lead frame assembly, and an optical field flattener. The lead frame assembly is an insulating rectangle through which the electrical connections to the detector and a thermoelectric cooler (TEC) pass. The field flattener is a plano-concave sapphire window. The purpose of the field flattener, in addition to providing a window to the sealed CCD package, is to further increase the radius of curvature of the focal field and coincide better with the planar CCD array.

Mounted to the backside of the field flattener are three order-sorting filters that provide the out-of-band rejection of light diffracted towards the focal plane assembly from other grating orders. The CCD is mounted to a TEC that is, in turn, mounted to the base plate heat sink. The CCD is designed with built-in thermistors that are part of an active temperature control system to meet the stability and end-of-life dark current requirements. The detector assembly has been included in the stray light analysis of the spectrometer, which showed that a significant reduction in the amount of scattered light could be achieved by rotating the CCD about its long axis by 11 degrees and eliminating internal reflections within the detector assembly. Also within the detector assembly is the InGaAs photodiode for the 1540 nm channel. This channel lies in the zero-order beam and has its band pass determined by a filter in much the same manner as was done with two of the channels in SAGE II. This detector is within the assembly because of the close proximity of the zero-order light rays to the end of the CCD array. Prototype detectors have been manufactured and tested for spectral quantum efficiency, dark current versus temperature, full-well capacity, charge transfer efficiency, and linearity. Radiation testing with monoenergetic proton beams of differing total doses have assessed the performance in a radiation environment, and led to models of energetic particle transport and secondary particle production, and an assessment of the shielding requirements for the CCD. In addition, models were developed to describe the observed temperature dependent gain of the field effect transistor preamplifiers on the CCD.

The spectrometer with the CCD array of detectors provides continuous wavelength coverage between 280 and 1040 nm and will permit the measurement of multiple absorption features of each gaseous species and multi-wavelength measurements of broadband extinction by aerosols. In the present configuration, 12 solar channels (≤ 80 sub-channels) will be routinely utilized in the solar occultation measurements and 3 channels (340 sub-channels) in the lunar occultation measurements, greatly decreasing the random error in the measurements (precision), and allowing for more accurate modeling of the multi-wavelength aerosol extinction. Included within the instrument band pass is the O₂ A-band (around 760 nm) which will permit the retrieval of density and temperature with which the viewing geometry (as a pressure level) can be inferred. This improvement over SAGE II, which relied upon the NOAA gridded analyses, should improve the accuracy of the SAGE III profiles and simplify the comparison with other measurements. Additionally, the linear array of detectors will permit on-orbit wavelength and intensity calibration from observations of the exoatmospheric solar Fraunhofer spectrum. The continuous spectral calibration, combined with the self-calibrating nature of the occultation technique (ratioing the signal transmitted through the atmosphere to the exoatmospheric reference signal for each measurement) makes SAGE III ideal for long-term monitoring of trends in ozone and other gas species, which is a central objective of the EOS program.

The expanded spectral coverage of the SAGE III instrument permits the observation of O₃ in the mesosphere between 65 and 85 km by utilizing the UV absorption in the short wavelength region between 385 and 290 nm and, combined with a fixed channel InGaAs detector at 1550 nm, should greatly enhance the characterization of multi-wavelength aerosol and clouds and extend this capability to lower altitudes in the troposphere. The

CCD array will provide approximately 2-nm resolution in the spectral region between 920 and 960 nm. In combination with an increase in digitization from 12 bit precision to 16 bit precision, this should allow for greater discrimination of water vapor from aerosol (both volcanic and thin cloud), and better retrieval of the higher water vapor values at lower altitudes in the troposphere than was possible with SAGE II. Table A.1 details the measurement capability of SAGE III for single profile retrievals. The notable difference, as discussed above, is the determination of pressure and temperature from oxygen A-band and the improved precision from the inclusion of additional channels.

With a 16-bit A/D converter, the SAGE III spectrometer will allow for variable integration time and on-orbit gain programming necessary for lunar observations. This potentially doubles the number of measurements per orbit, but requires a detector and signal chain that can accommodate the reduced flux observed during lunar occultations. In lunar occultation SAGE III will monitor O₃, NO₂, pressure, and H₂O, as well as OCIO and NO₃.

Table A.1: SAGE III measurement capability (single profile)

Channel	Wavelength (nm)	Products	Solar Altitude	Error (%)	Lunar Altitude (km)	Error (%)
S1	290	O ₃	50-85	10	----	----
S2	385	Aerosol	15-40	10	----	----
L1	380-420	OCIO	----	----	15-25	25
S3/L1	433-450	NO ₂ , Aerosol	10-50, 10-40	15 ----	20-50	10
L1	470-490	O ₃	----	----	16-35	10
S4	521	Aerosol, Cloud	6-40	10 ----	----	----
S5	560-616	O ₃	6-60	5	----	----
L1	640-680	NO ₃	----	----	20-55	10
S6	670	Aerosol	3-40	5	----	----
S7	758	Aerosol	3-40	5	----	----
S8/L2	759-771	Pressure, Temperature	0-85, 0-85	2 2K	----	----
S9	869	Aerosol	0-40	5	----	----
S10/L3	933-960	H ₂ O,	0-50,	15	----	----
S11	1020	Aerosol, Cloud	0-40	5	----	----
S12	1540	Aerosol, Cloud	0-40	5	----	----

- a. Error is estimated precision
- b. Lowest altitude is determined by cloud top height

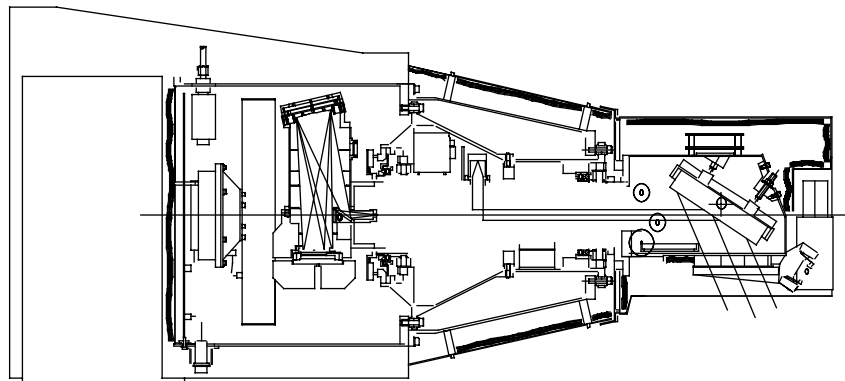


Figure A.1. The SAGE III sensor assembly.

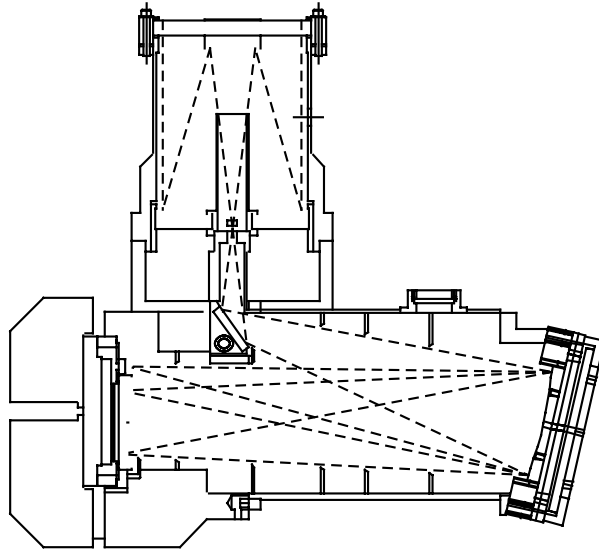
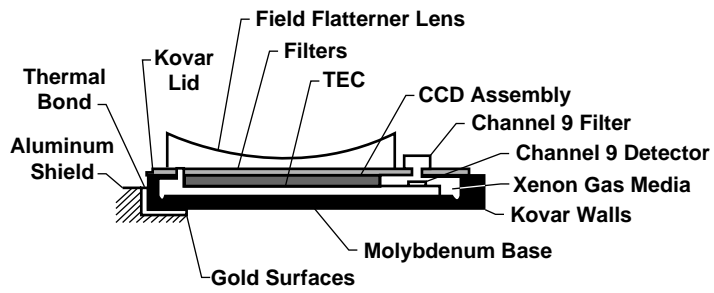


Figure A.2. Optical configuration and ray paths for the SAGE III telescope and spectrometer.

Side Section View



End Section View

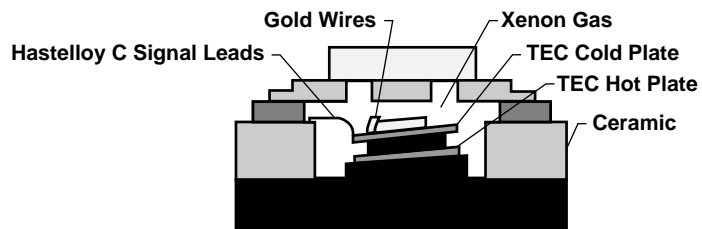


Figure A3. SAGE III detector package.

Appendix B. Atmospheric Inhomogeneity

The SAGE III inversion algorithm, as do essentially all processing algorithms for limb viewing instruments, assumes that the atmosphere is spherically homogeneous. This is probably a good assumption for most stratospheric constituents but is not always true for cloud and may well be a poor approximation for other constituents in the troposphere. Of all the species measured by SAGE III, cloud is most likely to be affected by its own inhomogeneous nature. Despite this, the current SAGE III algorithm, essentially an extension of that used for SAGE II [Kent *et al.*, 1993], neglects this feature of cloud observations. Simulation studies are in progress that may lead to modifications in the cloud detection algorithm that exploit inhomogeneity as a tool to infer the presence of cloud. Inhomogeneous cloud, whether stratospheric or tropospheric, is likely to degrade the quality of concurrent SAGE III measurements of molecular species and temperature and pressure.

Airborne lidar data, taken on an approximately 8000 km flight path over the tropical Pacific, has been used to simulate high altitude SAGE II cloud measurements and their inversion [Kent *et al.*, 1997]. These simulations produce cloud extinction values similar in magnitude and distribution to those obtained from SAGE II. They also show the existence of three possible error conditions that result from the inhomogeneous nature of the cloud:

1. The true altitude of a cloud may be higher than that found as a result of the SAGE II inversion. Errors of 1 km or more occurred in ~40% of the data set.
2. The inverted cloud extinction may differ (biased low) from the volume averaged extinction along the horizontal ray path.
3. The presence of non-uniform or isolated cloud patches can result in an apparent negative inverted extinction value just below the cloud. Such values were observed in about one third of the simulations. The present SAGE II inversion scheme (bottom up Twomey-Chahine) suppresses these negative values but compensates by reducing the extinction value just above the offending level.

SAGE transmission measurements are an amalgamation of several independent scans across the Sun. In the presence of cloud or other inhomogeneities, these scans will measure different amounts of transmitted radiation from the same point on the Sun (because the spacecraft moves and the LOS at a given tangent altitude, as a result, also moves). These differences are manifested in the transmission data as an increased standard deviation relative to homogeneous conditions. The possibility exists that this variability may be used as an additional input to the cloud detection algorithm. The simulation described above has been extended to include spacecraft motion and compared to results from SAGE II observations.

Figure B.1 shows a scatter plot of SAGE II data at an altitude of 14.5 km in which the relative error in the slant path optical depth (SPOD) has been plotted against the SPOD

itself. Low values of SPOD, corresponding to cloud-free observations, show low relative error. As cloud is observed in some scans, the relative error increases to a maximum as SPOD also increases. Then as more and more scans observe cloud, the relative error decreases as SPOD continues to increase. Figure B.2 shows the equivalent simulation using airborne lidar data. The behavior is very similar to that shown in Figure B.1. Individual data points in this figure are coded by their wavelength extinction ratio (525 to 1020 nm aerosol extinction ratio). This ratio is used as the primary discriminator between cloud and aerosol in SAGE II observations and is similar to that proposed for the SAGE III algorithm. We note that the majority of the high error cases (mixed cloud) would be identified as cloud due to their low extinction ratio. However, some high error cases have higher extinction ratios and would not be identified as cloud by the SAGE II algorithm though cloud is clearly present.

Based on these results, we plan to carry out further simulations of the effect of cloud and other inhomogeneities on the inversion algorithm and data quality (not only on cloud presence but also for all other detected species). In particular, we will investigate the effects of Polar Stratospheric Clouds (PSCs) on data from the SAGE III/METEOR 3M flight. The outcome of further simulations may lead to modifications of the inversion algorithm (particularly for cloud detection) and error estimation. We will also consider the implication of cloud homogeneity on the SAGE III validation program (particularly its tropospheric section).

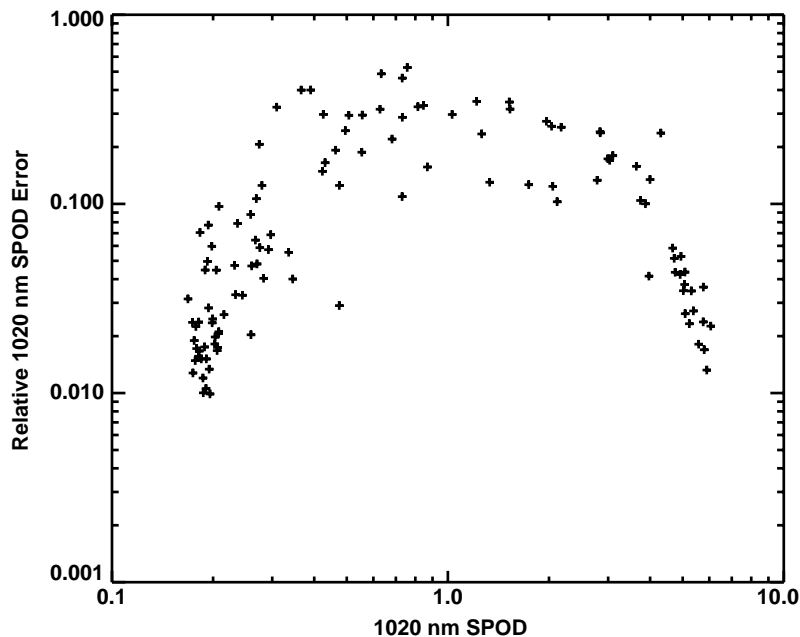


Figure B.1 A scatter plot of SAGE II data at an altitude of 14.5 km, in which the relative error in the slant path optical depth (SPOD) is plotted against the SPOD itself. Data points cover both cloudy and non-cloudy situations.

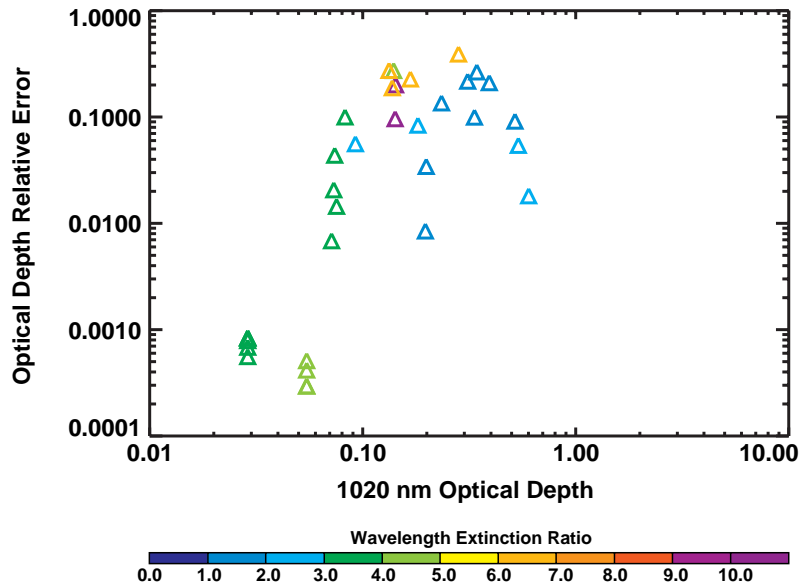


Figure B.2 Scatter plot equivalent to that shown in figure E.1, but derived from simulations based on airborne lidar data obtained within a cloud field. The color coding shows the retrieved 525 to 1020-nm aerosol extinction ratio.

References

Kent, G. S., D. M. Winker, M. T. Osborn and K. M. Skeens, A model for the separation of cloud and aerosol in SAGE II occultation data, *J. Geophys. Res.*, 98, 20725-20735, 1993.

Kent, G. S., D. M. Winker, M. A. Vaughan, P-H. Wang, and K. M. Skeens, Simulation of SAGE II cloud measurements using airborne lidar data. *J. Geophys. Res.*, 102, 21,795-21,807, 1997.

Appendix C. Molecular Absorption Cross-Sections: Spectroscopic Considerations for SAGE III

C.1 Introduction

This appendix reviews the current knowledge of molecular absorption cross sections as it pertains to the SAGE III instrument, and is focused on the spectroscopic needs of the planned SAGE III measurements. This means the discussion is limited to those molecules and spectral regions that will be measured by the SAGE III instrument. Each of the individual molecules measured by SAGE III is discussed in a separate sections. However, each section addresses not only that part of the spectrum which is used to measure that gas but the rest of the spectrum where absorption by that species could interfere with the retrieval of other molecules.

Since new spectroscopic measurements will be conducted over the lifetime of SAGE III operation, improvement in the molecular absorption cross-section database will evolve with time. Therefore, the SAGE III software will utilize the most up-to-date spectroscopic data for processing and generation of SAGE III products.

C.2 Species Specific Information

C.2.1 Ozone

C.2.1.1 Ultraviolet

Recent Measurements

The compilation of UV ozone cross-sections for LOWTRAN 7 and MODTRAN, by G.P. Anderson *et al.* [1989] is currently recommended, at least for wavelengths up to 345 nm. This compilation is primarily based on the data of Bass and Paur [1985] from 240 to 330, including a quadratic temperature dependence. Between 180 and 240 nm the measurements of Molina and Molina [1986] are used. The measurements of Molina & Molina [1986] and Yoshino *et al.* [1988] were used to extend the temperature dependent range to 340 nm, and preliminary data of Cacciani *et al.* [1987], (later published as Cacciani *et al.* [1989]), was to extend the wavelength coverage to 365 nm.

For wavelengths from 345 to 354 nm, the room temperature values in MODTRAN are consistent with those of Molina & Molina [1986] and with those of Cacciani *et al.* [1989]. However there appears to be a problem with their temperature dependence for wavelengths greater than 345, resulting in a significant underestimate of the ozone

absorption at stratospheric temperatures. The cause of this problem with the temperature dependence is not clear, (G. P. Anderson, private communication, 1996).

The recent room temperature measurements by Daumont *et al.* [1992] from 195 to 345 nm, agree within the stated accuracies with these earlier values. This group recently has extended these measurements to lower temperatures, [Malicet *et al.*, 1998]. Burrows *et al.* [1999] have also measured the temperature dependence of ozone from 231 to 794 nm. These measurements, along with the recent accurate measurements of the ozone cross section for the 253.7 nm mercury line, by the University of Minnesota Group [Mauersberger, *et al.* 1986 and 1987; and Barnes and Mauersberger, 1986], should be used to re-examine the cross sections for this whole spectral region. The cross section at this mercury line based on Hearn's [1961] data was used to normalize the Bass and Paur [1985] data, along with a number of the earlier measurements.

Brion *et al.*, [1998] have preliminary results continuing the room temperature measurements for ozone absorption from 345 nm to 830 nm. These should be used to extend the ozone cross sections through the gap that currently exists in the available quantitative data between 360 and 410 nm.

Estimated Accuracy

The uncertainties in the UV data are generally within 1 to 2 % for wavelengths less than 325 nm. At longer wavelengths the uncertainties become increasingly larger as the values of the absorption cross section become smaller with increasing wavelength, and the uncertainties in the zero-absorption reference value become more significant. The uncertainties are nearly 10% by 345 nm, and greater than 20% for wavelengths greater than 350 nm. In the vicinity of the absorption minimum near the SAGE 385 nm aerosol channel, the uncertainties in the absorption cross section exceeds a factor of 2. However, at this wavelength the ozone absorption is negligible compared to the aerosol attenuation and is less than 5% of the typical aerosol extinction near 30 km (and the peak ozone mixing ratio).

C.2.1.2 Visible and Near Infrared Cross-Sections:

Recent Measurements

Recently there have been several new spectroscopic studies of the ozone Chappuis and Wulf absorption bands, [Anderson *et al.*, 1990, 1991, 1993a, and Burkholder and Talukdar, 1994] along with measurements of the absolute cross section at selected wavelengths near the peak of the Chappuis band, [Anderson and Mauersberger, 1992], and in the near IR, [Anderson *et al.*, 1993b]. Shettle and Anderson [1994] have used these to develop a new set of room temperature ozone absorption cross-sections. They

normalized the spectral measurements to agree with the absolute cross-section data, within the measurement uncertainties, and smoothly joined the different sets of measurements, to provide the new cross-section over the spectral range from 407 to 1089 nm.

Burkholder and Talukdar [1994] have provided a very nice measurement of the temperature dependence of the Chappuis band [from 407 to 762 nm], where they use two identical cells to directly measure the ratio of the cross sections at 298 K and a reduced temperature between 220 and 280 K.

Estimated Accuracy

The accuracy of this data set is about 1 to 2% from about 520 nm through 800 nm, where the cross sections can be constrained by the measurements of Anderson and Mauersberger, [1992], and of Anderson *et al.*, [1993b]. At the extreme wavelengths near 407 and 1089 nm, where the cross section becomes very small the uncertainties are driven by sensitivity of the measurements and possible errors in the zero absorption reference value. Near these wavelengths the uncertainties in the data can exceed 25%, decreasing to 10% near 450 nm and to less than 5% near 500 nm. At the longer wavelengths, the uncertainties in the ozone cross sections increase from 2% to 5% between 800 and 850 nm, with a further increase to about 10% near 950 nm. The recent results of Brion *et al.* [1998], tend to be systematically higher by 1% than the measurements discussed above.

Burkholder and Talukdar [1994] have provided a very nice measurement of the temperature dependence of the Chappuis band [from 407 to 762 nm], where they use two identical cells to directly measure the ratio of the cross sections at 298 K and a reduced temperature between 220 and 280 K.

Deficiency of Current Available Measurements

The most significant deficiencies in the ozone data for SAGE III are the need to extend the measurements of the temperature dependence to 180 K, to cover the full range of stratospheric temperatures and through the near IR. The latter is needed more to remove ozone as an interfering species from the SAGE measurement of aerosols and water vapor in the near IR as directly to measure ozone. While Burrows *et al.* [1999] have measured the temperature dependence in out to 794 nm, their room temperature data is systematically higher than either the Shettle and Anderson [1994] compilation or the Brion *et al.* [1998] measurements throughout the visible. These differences range from 3 to 5 % near the 600 nm Chappuis peak, to in excess of 20% near 750 nm. Also the Burrows *et al.* [1998] temperature dependence in the visible shows internal inconsistencies.

C.2.1.3 References

- Anderson, G. P., F. X. Kneizys, E. P. Shettle, L. W. Abreu, J. H. Chetwynd, R. E. Huffman, and L. A. Hall, UV Spectral Simulations Using LOWTRAN 7, in *Atmospheric Propagation in the UV, Visible, IR, & MM-Wave Region and Related Systems Aspects*, AGARD Conference Proceedings No. 454, Proceedings of the AGARD Electromagnetic Wave Propagation Panel Symposium Copenhagen, Denmark, 9-13 October 1989.
- Anderson, S. M., P. Hupalo, and K. Mauersberger, Rotational structure in the near-infrared absorption spectrum of ozone, *J. Chem. Phys.*, 99, 737-739, 1993a.
- Anderson, S. M., P. Hupalo, and K. Mauersberger, Ozone absorption cross section measurements in the Wulf bands, *Geophys. Res. Lett.*, 20, 1579-582, 1993b.
- Anderson, S. M., J. Maeder, and K. Mauersberger, Effect of isotopic substitution on the visible absorption spectrum of ozone, *J. Chem. Phys.*, 94, 6351-6357, 1991.
- Anderson, S. M. and K. Mauersberger, Laser measurements of ozone absorption cross sections in the Chappuis band, *Geophys. Res. Lett.*, 19, 933-936, 1992.
- Anderson, S. M., J. Morton, and K. Mauersberger, "Near-infrared absorption spectra of $^{16}\text{O}_3$ and $^{18}\text{O}_3$: Adiabatic energy of the $^1\text{A}_2$ state?", *J. Chem. Phys.*, 93, 3826-3832, 1990.
- Barnes, J. and K. Mauersberger, Temperature Dependence of the Ozone Absorption Cross Section at the 253.7-nm Mercury Line, *J. Geophys. Res.*, 92, 14,861-14,864, 1987
- Bass, A. M. and R. J. Paur, The ultraviolet Cross-Sections of Ozone. I. Measurements in Atmospheric Ozone, *Proceedings of the Quadrennial Ozone Symposium in Halikidi, Greece*, ed. by C. Zeferos and A. Ghaz, pp 606-616, 1985.
- Brion, J. A. Chakir, J. Charbonnier, D. Daumont, C. Parisee, J. Malicet (X), Absorption Spectra Measurements for the Ozone Molecule in the 350 to 830 nm Region, *J. Atmos. Chem.*, 30, 291-299, 1985
- Burkholder, J. B. and R. K. Talukdar, Temperature dependence of the ozone absorption spectrum over the wavelength range 410 to 760 nm, *Geophys. Res. Lett.*, 21, 581-584, 1994.
- Burrows, J.P., A. Richter, A. Dehn, B. Deters, S. Himmelmann, S. Voigt, and J. Orphal, Atmospheric remote-sensing reference data from GOME – 2. Temperature-dependent

absorption cross sections of O₃ in the 231-794 nm range, *J. Quant. Spectrosc. Radiat. Transfer*, 61, 509-517, 1999.

Cacciani, M., A. diSarra, and G. Fiocco, Laboratory Measurements of the Ozone Absorption Coefficients in the Wavelength Region 339-362 nm at Different Temperatures, Dept. of Physics, University of Roma - La Sapienza, Italy, Internal Note No. 882, 1987.

Cacciani, M., A. diSarra, and G. Fiocco, and A. Amuruso, Absolute Determination of the Cross-Sections of Ozone in the Wavelength Region 339-355nm at Temperatures 220-293K, *J. Geophys. Res.*, 94, 8485-8490, 1989.

Daumont, D., J. Brion, J. Charbonnier, and J. Malicet, Ozone UV Spectroscopy I: Absorption Cross Sections at Room Temperature, *J. Atmos. Chem.*, 15, 145-155, 1992.

Malicet, J., D. Daumont, J. Charbonnier, C. Parisse, A. Chakir, and J. Brion, Ozone UV spectroscopy. II Absorption cross-sections and temperature dependence, *J. Atmos. Chem.*, 21, 263-273, 1995.

Mauersberger, K., J. Barnes, D. Hanson, and J. Morton, Measurement of the Ozone Absorption Cross Section at the 253.7 Mercury Line, *Geophys. Res. Lett.*, 13, 671-673, 1986.

Mauersberger, K., D. Hanson, J. Barnes, and J. Morton, Ozone Vapor Pressure and Absorption Cross Section Measurements: Introduction of an Ozone Standard, *J. Geophys. Res.*, 92, 8480-8485, 1987.

Molina, L. T. and M. J. Molina, Absolute Absorption Cross Sections of Ozone in the 185-350 nm Wavelength Range, *J. Geophys. Res.*, 91, 14,501-14,509, 1986.

Shettle, E. P. and S. M. Anderson, New Visible and Near IR Ozone Cross Sections for MODTRAN, presented at the 17th Annual Review Conference on Atmospheric Transmission Models, Phillips Laboratory, Bedford, MA 7-8 June 1994.

Yoshino, K. D.E.Freeman, J.R.Esmond, and W.H.Parkinson, Absolute Absorption Cross Section Measurements of Ozone in the Wavelength Region 238-335 nm and the Temperature Dependence, *Planet. Space Sci.*, 36, 395-398, 1988.

C.2.2 Nitrogen Dioxide

Recent Measurements

SAGE II has used the NO₂ cross sections measured by Graham and Johnston [1974] and compiled by Goldman *et al.* [1978] for their retrieval of the NO₂ profiles, [Cunnold *et al.*, 1991]. Since then there have been several new measurements of NO₂ absorption cross sections, [Schneider *et al.*, 1987; Davidson *et al.*, 1989; Amoruso *et al.*, 1993; Harwood and Jones, 1994; Mérienne *et al.*, 1995; and Coquart *et al.*, 1995]. Unfortunately intercomparisons of these different data sets with each other and the Graham and Johnston [1974] measurements show differences as large as 1 nm in the position of the minima and maxima of the absorption as a function of wavelength, in addition to differences of up to 10-20 % in the total cross section. One deficiency of many of these measurements (and most of the earlier ones) is they were made at resolutions of 0.5 to 2 nm which is too coarse to resolve the structure present in the absorption spectrum. Kirmse, *et al.* [1997] have concatenated several of these earlier measurements to develop a single NO₂ cross section covering 300 to 908 nm. Using the Mérienne *et al.* [1995] for the 300 to 500 nm region which includes the 420 to 460 nm region used by SAGE III for its NO₂ measurements.

Harder *et al.* [1997], provide a detailed critical evaluation of the earlier measurements, in addition to high spectral resolution (< 0.01 nm) data of their own, covering 350 to 585 nm, at temperatures between 217 and 298 K. These agree with the University of Reims data (by Courtuis) to about 4% in absolute cross section. The details of the spectral structure agree although the effects of the aliasing in the Reims data are clearly present.

Recently Yoshino *et al.* [1997] and Vandaele, *et al.* [1996 and 1998] have also made high spectral resolution (< 0.1 nm) measurements of the NO₂ cross sections. These all show agreement with the high resolution data of Mérienne *et al.* [1995] and Harder *et al.* [1997], to 3 to 5 %. Most of these results include at least one low temperature measurement (except Yoshino *et al.*, 1997). These low temperature measurement also agree to within 5%, with the spectral variations becoming more pronounced. That is the local minima decrease with decreasing temperature and the local maxima increase with decreasing temperature.

Estimated Accuracy

With an instrument such as SAGE II which uses the difference between a single minimum and maximum, the use of a pair where there are large differences between the positions and cross sections, could lead to errors as large as 50 % by using the wrong cross section data. It should be noted that the validation of the SAGE II NO₂ measurements, [Cunnold *et al.*, 1991], indicate that the SAGE NO₂ data is accurate to 15%. SAGE III will retrieve the NO₂ from the structure across several minima and

maxima, which should mean it is much less sensitive to the position and cross sections of individual pairs of the minima and maxima. In fact the SAGE III spectral measurements can be used to check for systematic wavelength shifts in the NO₂ absorption data used in the algorithm.

In the spectral region from 400 nm to 460 nm, where there are a number of good quality high resolution measurements available, the uncertainties in the NO₂ absorption cross sections are 3-5 %. This includes the portion of the spectrum used by SAGE III and many other instruments to determine the concentration of NO₂ in the atmosphere. From 300 nm to 400 nm and from 460 nm to 500 nm the uncertainties are 5-7 %. At longer wavelengths, which are still important to remove the contributions of NO₂ from the measurements of other species such as aerosols or NO₃, the uncertainties are 5-10 %, and are limited to measurements with resolutions (and wavelength accuracies) of 0.5 to 2 nm, which means additional errors will be introduced in convolving them with the spectral response of the SAGE III instrument. The greatest needs for additional measurements are for high resolution data at wavelengths longer than 500 nm and for low temperature measurements at all wavelengths down to 180 K, to cover the full range of stratospheric temperatures.

C.2.2.1 References

- Amoruso, A. L., G. Crescentini, G. Fiocco, and M. Volpe, New Measurements of the NO₂ Absorption Cross Section in the 440- to 460- nm region and estimates of the NO₂ - N₂O₄ Equilibrium Constant, *J. Geophys. Res.*, 98, 16,857-16,863, 1993.
- Bass, A. M., A. E. Ledford Jr., and A. H. Laufer, Extinction Coefficients of NO₂ and N₂O₄, *J. Res. Natl. Bur. Stand.*, 80A, 143-166.
- Coquart, B. A. Jenouvrier, and M. F. Mérienne, The NO₂ Absorption Spectrum. II: Absorption Cross-Sections at Low Temperature in the 400-500 nm Region, *J. Atmos. Chem.*, 21, 251-261. 1995.
- Cunnold, D. M., J. M. Zwadony, W. P. Chu, J. P. Pommereau, F. Goutail, J. Lenoble, M. P. McCormick, R. E. Viegas, D. Murcray, N. Iwagami, K. Shibasaki, P. C. Simon, and W. Peetermans, Validation of SAGE II NO₂ Measurements, *J. Geophys. Res.*, 96, 12,913-12,925, 1991.
- Davidson, J. A., C. A. Cantell, A. H. McDaniel, R. E. Shetter, S. Madronich, and J. G. Calvert, Visible-Ultraviolet Absorption Cross Sections for NO₂ as a Function of Temperature, *J. Geophys. Res.*, 93, 7105-7112, 1989.

- Frost, G. J., L. M. Goss, and V. Vaida, Measurements of High-Resolution Ultraviolet-Visible absorption Cross Sections at Stratospheric Temperatures: 1. Nitrogen Dioxide, *J. Geophys. Res.*, 101, 3869-3877, 1996.
- Graham, R. and H.S. Johnston, Photochemistry of NO_x and HNO_x Compounds, *Can. J. Chem.*, 52, 1415-1423, 1974. [Values tabulated by A. Goldman, U. of Denver]
- Hall, T. C. and F. E. Blacet, Separation of the Absorption Spectra of NO₂ and N₂O₄ in the range 2400-5000 D, *J. Chem. Phys.*, 20, 1745-1749, 1952.
- Harder, J. W. J. W. Brault, P. V. Johnston, and G. H. Mount, Temperature Dependent NO₂ Cross Sections at High Spectral Resolution, *J. Geophys. Res.*, 102, 3861-3879, 1997.
- Harwood, M. H. and R. L. Jones, Temperature Dependent Ultraviolet-Visible Absorption Cross-Sections of NO₂ and N₂O₄: Low-Temperature Measurements of the Equilibrium Constant for 2NO₂ ⇌ N₂O₄, *J. Geophys. Res.*, 99, 22,955-22,964, 1994.
- Mérienne, M. F., A. Jenouvrier, B. Coquart, The NO₂ Absorption Spectrum. I: Absorption Cross-Sections at Ambient Temperature in the 300-500 nm Region, *J. Atmos. Chem.*, 20, 281-297, 1995.
- Schneider, W. G., G. K. Moortgat, G. S. Tyndall, and J. P. Burrows, Absorption Cross Sections of NO₂ in the UV and Visible Region (200-700 nm) at 298 K, *J. Photochem. Photobiol. A Chem.*, 40, 195-217, 1987.
- Vandaele, A. C., C. Hermans, P. C. Simon, M. Carleer, R. Colin, S. Fally, M. F. Merienne, A. Jenouvrier, and B. Coquart, Measurements of the NO₂ absorption cross-sections from 42,000 cm⁻¹ to 10,000 cm⁻¹ (238-1000 nm) at 220 K and 294 K, *J. Quant. Spectrosc. Radiat. Transfer*, 59, 171-184, 1998.
- Yoshino, K., J. R. Esmond, W. H. Parkinson, High-resolution absorption cross section measurements of NO₂ in the UV and visible region, *Chem. Phys.*, 221, 169-174, 1997.

C.2.3 Oxygen

Accurate knowledge of the oxygen absorption cross sections is critical for the SAGE III Experiment, since the SAGE III oxygen measurements are used to establish the atmospheric density, temperature, and pressure profiles. In addition to the direct scientific need for these profiles, they are also needed to remove the molecular Rayleigh scattering contribution from the measurements of other species at all wavelengths, and for the retrieval of the mixing ratio of the other gaseous species on pressure surfaces. This

removes the need for an external source of this data, such as the NMC analyses which were used for the SAGE I and II instruments. To retrieve the oxygen density, from which the atmospheric density, temperature, and pressure profiles will be derived, SAGE III will use differential absorption measurements across the oxygen A-band from 755 to 775 nm.

The Ritter and Wilkerson [1986] measurements of the oxygen A-band with a stated accuracy of about 2%, appear to be the best of the available data. They have been adapted by Chance [1995] for use with the Global Ozone Monitoring Experiment (GOME). However, their band strength is higher than all of the previous measurements that they include in their Table IV, exceeding the next highest by nearly 5%, the mean by 11%, and exceeding by 15% the data of Miller *et al.* [1969], (with a stated accuracy of 4%), which are the basis of the 1992 HITRAN database, [Rothman *et al.*, 1992]. Ritter and Wilkerson's [1986] line widths are near the middle of the range of the previous measurements, which have a 30% range of values. However, while the 1996 HITRAN database adapted the Ritter and Wilkerson [1986] line strengths, it continues to utilize the line widths of Givers *et al.* [1974], which are at the low end of the available measurements.

Recently Brown and Plymate [1999] have measured the oxygen A-band. The line positions, line intensities and pressure-broadening coefficients of 44 transitions in the oxygen A-band near 760 nm (from 13040 to 13168 cm^{-1}) have been calibrated using laboratory data recorded at 0.02 cm^{-1} resolution with the Fourier transform spectrometer at Kitt Peak in Arizona. The pressure-broadening coefficients for self-broadened and nitrogen-broadened widths and pressure-induced shifts in line positions have been measured through $J'' = 24$; these have been combined and modeled with a polynomial expressed as a function of the upper state quantum number in order to compute the corresponding air-broadened line shape coefficients associated with Voigt profiles. The temperature dependence of the line widths has been determined from absorption spectra obtained with gas samples temperatures between 205 K and 297 K.

The measured intensities demonstrate that the values selected for the 1996 HITRAN database are valid to within 1%. However, the line positions are in error by 0.002 to 0.015 cm^{-1} and the widths by 7 to 20%. Although the individual new measurements of temperature dependence of widths have uncertainties of 15%, the average of new measured values is within 2% of the mean value previously selected by HITRAN.

C.2.3.1 References

Brown, L. R. and C. Plymate, Experimental line parameters of the oxygen A-band at 760 nm., *submitted to J. Mol. Spectrosc.*, 1999.

Brown, L. R. and R. A. Toth, Laboratory Spectroscopy of SAGE Molecules, Unpublished Manuscript, 1995.

Chance, K., O₂ A-band Studies for Cloud Detection and Algorithm Improvement, Contact Report for ESA, 1995.

Giver, L. P., R. W. Boese, and J. H. Miller, Intensity Measurements, Self-Broadening Coefficients, and Rotational Intensity Distribution for Lines of the Oxygen B Band at 6880 C, *J. Quant. Spectrosc. Radiat. Transfer*, 14, 793-802, 1974.

Miller, J. H., R. W. Boese, and L. P. Giver, Intensity Measurements and Rotational Intensity Distribution for the Oxygen A-band, *J. Quant. Spectrosc. Radiat. Transfer*, 9, 1507-1517, 1969.

Newnham, D. A., and J. Ballard, Visible absorption cross sections and integrated absorption intensities of molecular oxygen (O₂ and O₄), *J. Geophys. Res.*, 103, 28,801-28,816, 1998.

Ritter, K. J. and T. D. Wilkerson, High Resolution Spectroscopy of the Oxygen A-band, *J. Molec. Spectrosc.*, 121, 1-19, 1987.

Rothman, L. S., R. R. Gamache, R. H. Tipping, C. P. Rinsland, M. A. H. Smith, D. C. Benner, V. M. Devi, J.-M. Flaud, C. Camy-Peyret, A. Perrin, A. Goldman, S. T. Massie, L. R. Brown, and R. A. Toth, The HITRAN Molecular Database Editions of 1991 and 1992, *J. Quant. Spectrosc. Radiat. Transfer*, 48, 469-507, 1992.

Rothman, L. S. C. P. Rinsland, A. Goldman, S. T. Massie, D. P. Edwards, J.-M. Flaud, A. Perrin, C. Camy-Peyret, V. Dana, J.-Y. Mandin, J. Schroeder, A. McCann, R. R. Gamache, R. B. Watson, K. Yoshino, K. V. Chance, K. W. Jucks, L. R. Brown, V. Nemtchinov, and P. Varanasi, The HITRAN molecular spectroscopic database and HAWKS (HITRAN Atmospheric WorkStation): 1996 edition, *J. Quant. Spectrosc. Radiat. Transfer*, 60, 665-710, 1998.

C.2.4 Water Vapor

To measure atmospheric water vapor SAGE III will use differential absorption in the near IR water band from 920 to 960 nm. The HITRAN database, Rothman [1992], based on the measurements of Chevillard *et al.* [1989], provides the best available spectroscopic data, in this region. This is an improvement over the 1982 edition of the HITRAN database used by Chu *et al.* [1993] for the water vapor retrievals from SAGE II. However, as noted by Brown and Toth [1995], this band is a complex of 10 interacting vibrational states and a complete theoretical modeling has not been accomplished to date, limiting the ability to give a complete accurate listing of the line positions, intensities,

and spectral assignments. Recently Giver *et al.* [1999] have reported that there were systematic errors in implementing the line intensities of water vapor into the HITRAN database, which affects all the visible and near IR water bands with wavelengths less than 1200 nm. For the band centered around 940 nm, which will be used by SAGE III to retrieve water vapor, this correction amounts to a 14.4 % increase in all the lines derived from the data of Chevillard *et al.* [1989], which applies to most of the lines in this band. There are a number of weak lines in this region due to H₂¹⁷O and H₂¹⁸O, and a few unassigned lines. It is presently not clear whether this correction applies to any of these lines, however altogether they contribute only about 1% of the total band strength.

The reported accuracies of the Chevillard *et al.* [1989] data are 7 to 50 %, depending on the spectral line. Given the 50 % uncertainties apply to the weakest lines, when integrated over the 2 nm resolution of the SAGE III detector, the water vapor absorption is known to about 10 to 15 %. To achieve greater accuracy for water vapor retrievals will require new measurements of the water vapor spectroscopy in the near IR.

Recently Brown *et al.* [1999, unpublished manuscript], have obtained new measurements of the water vapor lines for the 940 nm band. The line positions and line intensities of some 2600 transitions have been retrieved from 17 absorption spectra recorded at 0.01 and 0.02 cm⁻¹ resolution using the Fourier transform spectrometer at Kitt Peak in Arizona. These have been combined with published analyses for isotopic water (H₂-¹⁶O-¹⁸O and H₂-¹⁶O-¹⁷O) to produce a new line list of some 4130 transitions from 9676.8789 to 11386.2119 cm⁻¹. Available air-broadened and self-broadened line widths from other vibrational bands at 6 μm and 2.1 μm have been inserted for A- and B- type transitions of bands in the 0.96 μm region. There are no new data for pressure-shifts and temperature dependences, however.

This study will correct the conversion mistakes recently uncovered in the visible line parameters of water by completely replacing the current 0.96 μm list in HITRAN and GEISA with better quality measurements (0.001 cm⁻¹ for positions and 3% for the intensities). The individual intensities range from 6.5 E⁻²² to 1.0 E⁻²⁷ cm⁻¹/(molecule cm⁻²) at 296 K.

C.2.4.1 References

Brown, L. R. and R. A. Toth, Laboratory Spectroscopy of SAGE Molecules, Unpublished Manuscript, 1995.

Chevillard, J.-P., J.-Y. Mandin, J.-M. Flaud, and C. Camy-Peyret, H₂¹⁶O: Line positions and intensities between 9500 and 11500 cm⁻¹. The interacting vibrational states (041), (220), (121), (022), 9300), (201), (102), and (003), *Can. J. Phys.*, 67, 1065-1084, 1989.

- Chu, W. P., E. W. Chiou, J. C. Larsen, L. W. Thomason, D. Rind, J. J. Buglia, S. Oltsman, M. P. McCormick, and L. M. McMaster, Algorithms and sensitivity analyses for Stratospheric Aerosol and Gas Experiment II water vapor retrieval, *J. Geophys. Res.*, 98, 4857-4866, 1993.
- Giver, L. P., C. Chackerian, and P. Varanasi, Visible and Near-Infrared H₂¹⁶O Line Intensity Corrections for HITRAN-96, *to be published in J. Quantat. Spectrosc. Radiative Transf.*, 1999.
- Rothman, L. S., R. R. Gamache, R. H. Tipping, C. P. Rinsland, M. A. H. Smith, D. C. Benner, V. M. Devi, J.-M. Flaud, C. Camy-Peyret, A. Perrin, A. Goldman, S. T. Massie, L. R. Brown, and R. A. Toth., The HITRAN Molecular Database Editions of 1991 and 1992, *J. Quant. Spectrosc. Radiat. Transfer*, 48, 469-507, 1992.
- Rothman, L. S., R. R. Gamache, A. Barbe, A. Goldman, J. R. Gillis, L. R. Brown, R. A. Toth, J.-M. Flaud, and C. Camy-Peyret, AFGL atmospheric absorption line parameters compilation: 1982 edition, *Appl. Opt.*, 22, 2247-2256, 1983.
- Rothman, L. S. C. P. Rinsland, A. Goldman, S. T. Massie, D. P. Edwards, J.-M. Flaud, A. Perrin, C. Camy-Peyret, V. Dana, J.-Y. Mandin, J. Schroeder, A. McCann, R. R. Gamache, R. B. Watson, K. Yoshino, K. V. Chance, K. W. Jucks, L. R. Brown, V. Nemtchinov, and P. Varanasi, The HITRAN molecular spectroscopic database and HAWKS (HITRAN Atmospheric WorkStation): 1996 edition, *J. Quant. Spectrosc. Radiat. Transfer*, 60, 665-710, 1998.

C.2.5 The Nitrate Free Radical NO₃

SAGE III utilizing differential absorption spectroscopy in the 640 to 680 nm region will measure the nitrate free radical NO₃. It is at least a weak absorber throughout the visible, although strong absorption features at 623 and 662 nm dominate its visible spectrum. A general review of the Nitrate Free Radical NO₃, including its spectroscopy, is given by Wayne *et al.* [1991].

DeMore *et al.* [1997] recommend using an average of the studies by Marinelli *et al.* [1982], Ravishankara & Wine [1983], Burrows *et al.* [1985], Ravishankara and Mauldin [1986], Sander [1986], Canosa-Mas *et al.* [1987], and Cantrell *et al.* [1987] for the cross section at the 662 nm peak at room temperature. There is disagreement in the temperature dependence with Cantrell *et al.* [1987] finding the absorption to be independent of temperature between 215 and 348 K, and Ravishankara and Mauldin [1986] and Sander [1986] reporting the cross section increasing with decreasing temperature. For the cross section increase, Ravishankara and Mauldin report 40 % between 298 and 220 K and Sanders 20 % between 298 and 230 K. The recent measurements of Yokelson *et al.* [1994] tend to support the temperature dependence of Sanders. Yokelson *et al.* also note

that their measurements can be considered to supersede the earlier results of Ravishankara & Mauldin [1987].

The uncertainties in the absorption cross sections are 10-15 % at room temperature and 20-25 % at stratospheric temperatures. Given this results in a corresponding uncertainty of the retrieved NO₃ amounts, improved measurements are needed.

C.2.5.1 References

Burrows, J. P., G. S. Tyndall, and G. K. Moortgat, Absorption spectrum of NO₃ and kinetics of the reactions of NO₃ with NO₂, Cl, and several stable atmospheric species at 298 K, *J. Chem. Phys.*, 89, 4848-4856, 1985.

Canosa-Mas, C. E., M. Fowles, P. J. Houghton, and R. P. Wayne, Absolute absorption cross section measurements on NO₃, *J. Chem. Soc. Faraday Trans. II*, 83, 1465-1474, 1987.

Cantrell, C. A., J. A. Davidson, R. E. Shetter, B. A. Anderson, and J. G. Calvert, The temperature Invariance of the NO₃ absorption cross section in the 662 nm region, *J. Phys. Chem.*, 91, 5858-5863, 1987.

DeMore, W. B., S. P. Sander, D. M. Golden, R. F. Hampson, M. J. Kurylo, C. J. Howard, A. R. Ravishankara, C. E. Kolb, and M. J. Molina, *Chemical Kinetics and Photochemical Data for Use in Stratospheric Modeling Evaluation Number 11*, JPL Publication 94-26, 1994.

DeMore, W. B., S. P. Sander, D. M. Golden, R. F. Hampson, M. J. Kurylo, C. J. Howard, A. R. Ravishankara, C. E. Kolb, M. J. Molina, *Chemical Kinetics and Photochemical Data for Use in Stratospheric Modeling Evaluation Number 12*, JPL Publication 97-4, 1997.

Marinelli, W. J., D. M. Swanson, and H. S. Johnston, Absorption cross sections and line shape for the NO₃ (0-0) band, *J. Chem. Phys.*, 76, 2864-2870, 1982.

Ravishankara, A. R. and R. L. Mauldin III, Temperature dependence of NO₃ cross section in the 662-nm region, *J. Geophys. Res.*, 91, 8709-8712, 1986.

Ravishankara, A. R. and P. H. Wine, Absorption Cross Sections for NO₃ between 565 and 673 nm, *Chem. Phys. Lettr.*, 101, 73-78, 1983.

Sanders, S.P. (1986) Temperature dependence of the NO₃ absorption spectrum, *J. Chem. Phys.*, 90, 4135-4142.

Wayne, R. P., I. Barnes, P. Biggs, J. P. Burrows, C. E. Canosa-Mas, J. Hjorth, G. Le Bras, G. K. Moortgat, D. Perner, G. Poulet, G. Restli, and H. Sidebottom, The Nitrate Radical: Physics, Chemistry, and the Atmosphere, *Atmos. Environ.*, 25A, 1-203, 1991.

Yokelson, R. J., J. B. Burkholder, R. W. Fox, R. K. Talukdar, and A. R. Ravishankara, Temperature Dependence of the NO₃ Absorption Spectrum, *J. Phys. Chem.*, 98, 13,144-150, 1994.

C.2.6 Symmetric Chlorine Dioxide OClO

Symmetric chlorine dioxide, OClO, has a series of absorption peaks between 280 and 480 nm, which reach a maximum near 351 nm. The region from 380 to 420 nm will be used for the SAGE III retrievals of OClO. While there have been a number of spectroscopic studies of OClO, relatively few experiments have provided absolute cross sections at room temperature, with apparently only Wahner *et al.* [1987] examining the temperature dependence. Frost *et al.* (1996) have recently reported a spectroscopic study of OClO at stratospheric temperatures (200 ± 20 K); however, using two different techniques to convert this data to absolute cross sections, report differences of 50%. DeMore *et al.* [1994] recommend the Wahner *et al.* [1987] absorption cross sections. These data have a reported accuracy of 3-5 %.

C.2.6.1 References

DeMore, W. B., S. P. Sander, D. M. Golden, R. F. Hampson, M. J. Kurylo, C. J. Howard, A. R. Ravishankara, C. E. Kolb, M. J. Molina, *Chemical Kinetics and Photochemical Data for Use in Stratospheric Modeling Evaluation Number 11*, JPL Publication 94-26, 1994.

Frost, G. J., L. M. Goss, and V. Vaida, Measurements of High-Resolution Ultraviolet-Visible absorption Cross Sections at Stratospheric Temperatures: 2. Chlorine dioxide, *J. Geophys. Res.*, 101, 3879-3884, 1996.

Wahner, A., G. S. Tyndall, and A. R. Ravishankara, Absorption cross sections for OClO as a function of temperature in the wavelength range 240-480 nm, *J. Phys. Chem.*, 91, 2734-2738, 1987.